University of Zurich[UZH]

Zurich Open Repository and Archive
University of Zurich
Main Library
Strickhofstrasse 39
CH-8057 Zurich
www.zora.uzh.ch

Year: 2020

Global sleep homeostasis reflects temporally and spatially integrated local cortical neuronal activity

Thomas, Christopher W ; Guillaumin, Mathilde C C ; McKillop, Laura E ; Achermann, Peter ; Vyazovskiy, Vladyslav V

Abstract: Sleep homeostasis manifests as a relative constancy of its daily amount and intensity. Theoretical descriptions define 'Process S', a variable with dynamics dependent on global sleep-wake history, and reflected in electroencephalogram (EEG) slow wave activity (SWA, 0.5–4 Hz) during sleep. The notion of sleep as a local, activity-dependent process suggests that activity history must be integrated to determine the dynamics of global Process S. Here, we developed novel mathematical models of Process S based on cortical activity recorded in freely behaving mice, describing local Process S as a function of the deviation of neuronal firing rates from a locally defined set-point, independent of global sleep-wake state. Averaging locally derived Processes S and their rate parameters yielded values resembling those obtained from EEG SWA and global vigilance states. We conclude that local Process S dynamics reflects neuronal activity integrated over time, and global Process S reflects local processes integrated over space.

DOI: https://doi.org/10.7554/elife.54148

Posted at the Zurich Open Repository and Archive, University of Zurich
ZORA URL: https://doi.org/10.5167/uzh-195932
Journal Article
Published Version

The following work is licensed under a Creative Commons: Attribution 4.0 International (CC BY 4.0) License.

Originally published at:
Thomas, Christopher W; Guillaumin, Mathilde C C; McKillop, Laura E; Achermann, Peter; Vyazovskiy, Vladyslav V (2020). Global sleep homeostasis reflects temporally and spatially integrated local cortical neuronal activity. eLife, 9:e54148.
DOI: https://doi.org/10.7554/elife.54148

RESEARCH ARTICLE

Global sleep homeostasis reflects temporally and spatially integrated local cortical neuronal activity

Christopher W Thomas[1], Mathilde CC Guillaumin[2], Laura E McKillop[1], Peter Achermann[3,4], Vladyslav V Vyazovskiy[1]*

[1]Department of Physiology, Anatomy and Genetics, University of Oxford, Oxford, United Kingdom; [2]Nuffield Department of Clinical Neurosciences, University of Oxford, Oxford, United Kingdom; [3]Institute of Pharmacology and Toxicology, University of Zurich, Zurich, Switzerland; [4]The KEY Institute for Brain-Mind Research, Department of Psychiatry, Psychotherapy and Psychosomatics, University Hospital of Psychiatry, Zurich, Switzerland

Abstract Sleep homeostasis manifests as a relative constancy of its daily amount and intensity. Theoretical descriptions define 'Process S', a variable with dynamics dependent on global sleep-wake history, and reflected in electroencephalogram (EEG) slow wave activity (SWA, 0.5–4 Hz) during sleep. The notion of sleep as a local, activity-dependent process suggests that activity history must be integrated to determine the dynamics of global Process S. Here, we developed novel mathematical models of Process S based on cortical activity recorded in freely behaving mice, describing local Process S as a function of the deviation of neuronal firing rates from a locally defined set-point, independent of global sleep-wake state. Averaging locally derived Processes S and their rate parameters yielded values resembling those obtained from EEG SWA and global vigilance states. We conclude that local Process S dynamics reflects neuronal activity integrated over time, and global Process S reflects local processes integrated over space.

***For correspondence:** vladyslav.vyazovskiy@dpag.ox.ac.uk

Competing interests: The authors declare that no competing interests exist.

Funding: See page 21

Received: 03 December 2019
Accepted: 19 June 2020
Published: 02 July 2020

Reviewing editor: Inna Slutsky, Tel Aviv University, Israel

© Copyright Thomas et al. This article is distributed under the terms of the Creative Commons Attribution License, which permits unrestricted use and redistribution provided that the original author and source are credited.

Introduction

According to traditional theory, the need for sleep accumulates during wakefulness and dissipates during sleep. Despite decades of research, it is still uncertain precisely which biological variables form the substrate of sleep need, what characteristics of wake challenge their stability, how information about sleep-wake history is integrated over time, and how sleep mediates the restoration of homeostasis. Daily sleep amount varies greatly across the animal kingdom, yet individuals generally perform a relatively constant and species-specific amount of sleep each day. An even more fundamental question therefore remains whether homeostatic sleep regulation reflects an active process, dynamically shaping daily sleep architecture in response to a physiological need for the homeostatic regulation of specific variables, or whether it corresponds instead to an unknown innate time-keeping process which ensures only that a certain daily quota of sleep is obtained.

The earliest theories of sleep homeostasis supposed the existence of a single variable, termed Process S, which describes sleep drive at the global level (***Borbély, 1982***). This variable is assumed to always increase during wakefulness, independently of its content, and to decline during sleep. It is widely acknowledged that homeostatic sleep pressure is reflected in the levels of slow wave activity (SWA, 0.5–4 Hz spectral power) observable during NREM sleep in neurophysiological field potentials, such as electroencephalogram (EEG) or local field potential (LFP). Although preceding sleep-wake history is considered a key determinant of sleep amount and intensity, the circadian process also plays an important role (***Daan et al., 1984***). It is thought that the master pacemaker of circadian

rhythmicity is located in the suprachiasmatic nucleus (SCN) of the hypothalamus, which consists of multiple cell-autonomous oscillators (**Hastings et al., 2019**). Although individual SCN cells may have widely diverse periods, the spatial averaging of their activities results in an occurrence of a stable circadian rhythm at the level of the whole animal (**Liu et al., 1997**; **Kunz and Achermann, 2003**).

Current views on the origin of sleep homeostasis emphasise the importance of a local and activity-dependent component (**Krueger and Tononi, 2011**; **Rattenborg et al., 2012**; **Tononi and Cirelli, 2014**). It was shown that SWA is far from uniform across the brain, and that the behavioural and cognitive content of waking, beyond its mere duration, influences subsequent sleep and cortical region-specific SWA (**Kattler et al., 1994**; **Huber et al., 2004**; **Vyazovskiy and Tobler, 2008**; **Rector et al., 2009**; **Murphy et al., 2011**; **Fisher et al., 2016**). Indeed, many candidate mechanisms for the substrate of sleep homeostasis implicate processes occurring at a cellular or local network level. These include the maintenance of cellular homeostasis (**Reimund, 1994**; **Mackiewicz et al., 2007**; **Vyazovskiy and Harris, 2013**; **Bellesi et al., 2016**), the replenishment of energy stores (**Scharf et al., 2008**), the influence of sleep-related signalling molecules such as adenosine or cytokines (**Krueger et al., 2008**), and the regulation of imbalanced synaptic strengths (**Tononi and Cirelli, 2003**; **Vyazovskiy et al., 2008**; **Liu et al., 2010**). Although the equivalence of these processes with Process S has not been conclusively demonstrated (**Frank and Heller, 2019**), the existing evidence supports the relevance of sleep-wake-dependent differences in neuronal activity for understanding the regulation of sleep.

Cortical neuronal activity is generally higher during waking compared to sleep (**Vyazovskiy et al., 2009**; **McKillop et al., 2018**), although this may depend on the cortical region (**Hengen et al., 2013**). Lower spike firing generally typical of sleep is thought to be due, at least in part, to regular periods of widespread synchronous network silence, termed off periods, intruding on ongoing activity (**Steriade et al., 1993b**; **Steriade et al., 2001**; **Sanchez-Vives and Mattia, 2014**). Importantly, off periods in neural populations are thought to underpin slow wave dynamics at the level of the field potential (**Steriade et al., 1993a**; **Massimini et al., 2004**; **Buzsáki et al., 2012**), and it was shown that their properties reflect homeostatic sleep need (**Vyazovskiy et al., 2009**; **McKillop et al., 2018**; **Saberi-Moghadam et al., 2018**).

Neuronal firing rates typically fluctuate around a homeostatic set point, which is characteristic for individual cells and variable across the population (**Turrigiano, 2011**; **Hengen et al., 2013**; **O'Leary et al., 2014**; **Styr et al., 2019**). The homeostatic regulation of firing rates may depend on processes occurring specifically in sleep and wakefulness (**Grosmark et al., 2012**; **Hengen et al., 2016**) and evidence suggests that firing rates change as a function of time spent awake, conditional on the behaviour (**Vyazovskiy et al., 2009**; **Fisher et al., 2016**). Additionally, the magnitude and direction of state-dependent changes in firing rate differs between neurons, depending on the brain region and their individual firing rate set point (**Hengen et al., 2013**; **Miyawaki and Diba, 2016**; **Watson et al., 2016**; **Miyawaki et al., 2019**). Firing rate homeostasis may occur above the individual cell level (**Slomowitz et al., 2015**), perhaps through synaptic plasticity induced by the sleep slow oscillation which may act to narrow the population firing rate distribution (**Levenstein et al., 2017**).

Overall, the evidence suggests that the homeostatic regulation of sleep and of neuronal firing rates may be intrinsically related, however, this functional link remains incompletely defined. Mathematical modelling approaches present an opportunity to address this problem. To this end, we developed novel quantitative models of Process S and demonstrated that its temporal dynamics, on both a local and global level, can be derived entirely from local neuronal activity, without any reference to the animal's sleep and wake states. We found that the magnitude of the deviation of multi-unit firing rate from a locally specified set point carries sufficient information to account for empirically derived patterns of SWA. We then introduced the total time spent in off periods as an alternative measure for Process S with more local origins than SWA, and showed how Process S dynamics may then be described in terms of two opponent processes, dependent on spiking rate and off period occurrence. Our data show that the global dynamics of Process S can be derived from a spatiotemporal integration of local neuronal activities. This suggests that a possible functional role for sleep homeostasis is to provide a precise intrinsic time-keeping mechanism.

Results

We analysed chronic recordings of the frontal electroencephalogram (EEG) alongside local field potential (LFP) and multi-unit activity (MUA) spiking from the primary motor cortex of six mice. These recordings were made continuously over 48 h, starting at light onset, while the mice were freely behaving within their cage and exposed to a standard 12 h - 12 h light-dark cycle. At light onset of the second day a sleep deprivation protocol was enforced for 6 h, involving the presentation of novel objects. Outside of this sleep deprivation period, mice were undisturbed and able to sleep at will.

Process S dynamics can be described as a function of vigilance state history

NREM sleep can be defined and distinguished from waking by the presence of high amplitude slow (0.5–4 Hz) waves in the EEG. The average EEG spectral power in the slow wave range (termed slow wave activity; SWA) in NREM sleep varies as a function of the animal's recent sleep-wake history, and this relationship has been captured in a classical quantitative theory using the concept of the homeostatic 'Process S' (**Borbély, 1982**; **Daan et al., 1984**). Process S describes a variable whose magnitude can be estimated from the level of SWA during NREM sleep, reflecting the intensity of sleep, and which is interpreted as corresponding to the homeostatic component of sleep drive (**Franken et al., 1991a**; **Achermann et al., 1993**; **Huber et al., 2000a**; **Vyazovskiy et al., 2007**; **Guillaumin et al., 2018**). Theoretically, Process S follows simple dynamics: during wake it increases according to a saturating exponential function towards an upper asymptote, while during NREM sleep it decays exponentially towards a lower asymptote. There are many published variants of the precise equations for this model, but, crucially, all these variants use the sleep-wake state history of the animal as the key predictive variable for Process S. Here, the specific equations used are:

$$\text{Wake/REM sleep}: \quad \frac{dS}{dt} = \alpha(S_{max} - S(t))$$

$$\text{NREM sleep}: \quad \frac{dS}{dt} = -\beta(S(t) - S_{min})$$

Where $S(t)$ represents the level of Process S as a function of time, S_{max} and S_{min} are upper and lower asymptotes, and α and β are rate parameters. The first equation is applied when the animal is scored to be awake or in REM sleep and the second equation is applied when it is scored to be in NREM sleep. Here, we use the typical approach of applying the wake dynamics equation to REM sleep (**Franken et al., 1991a**; **Huber et al., 2000a**; **Vyazovskiy et al., 2007**), but for simplicity do not set separate parameters for wake vs. REM sleep. For convenience, S is expressed in units equivalent to those of SWA. This classical formalism is later abbreviated as model Cl-SWA. Process S as described by these simple dynamics accounts for the time course of empirical SWA with high accuracy. We applied this model to SWA derived from the frontal EEG of all animals, and as expected obtained a high quality fit (**Figure 1A**).

Neuronal firing rates are associated with Process S dynamics and vigilance state distributions

Whichever specific processes within the brain underpin these state-dependent dynamics for Process S, we hypothesised that it is associated in some way to neuronal spiking activity, which differs characteristically between wake and NREM sleep (**Figure 1B**). The occurrence of spiking off periods causes firing rates to be typically lower during NREM sleep compared to wake and REM sleep. Consistent with this assumption, we found that the mean multi-unit firing rate averaged over all periods of wake was larger than the firing rate averaged over all periods of NREM sleep in every recording channel and every animal, with REM sleep showing typically intermediate values (**Figure 1C**).

Because the slow oscillation is underpinned by local neuronal dynamics, it is expected to be highly heterogeneous across the neocortex. Regional differences in SWA dynamics have been previously described, for example between frontal and occipital EEG derivations (**Werth et al., 1996**; **Huber et al., 2000b**), and can be accounted for within the classical Process S model through the selection of locally variable values for model rate parameters (**Zavada et al., 2009**; **Rusterholz and**

Figure 1. Cortical spike firing patterns are associated with the dynamics of Process S. (**A**) An example of the classical state-based Process S model (blue) describing the dynamics of frontal EEG SWA (median per NREM sleep episode, black bars) over 48 h in one representative animal. Sleep deprivation occurred as indicated at light onset of the second day and lasted 6 h. Scored vigilance states are also shown. (**B**) An example of frontal electroencephalogram (EEG), primary motor cortical local field potentials (LFP), corresponding raw signal with multi-unit activity (MUA) and detected spikes, in representative segments of waking and NREM sleep. Slow waves and synchronous spiking off periods are visible in NREM sleep but not in wakefulness. The y-scale is the same for both wake and NREM sleep plots. (**C**) The distribution (log scale) of mean firing rates during wake, NREM and

Figure 1 continued on next page

Figure 1 continued

REM sleep over all animals and channels, in addition to the difference in mean firing rates in wake compared to NREM sleep (all are positive, reflecting higher firing in wake). Points indicate channels grouped by animal (left to right), but boxplots reflect channels from all animals treated as one population. (**D**) Distribution of correlation coefficients, calculated within each single channel, between wake episode duration (Duration), the change in slow wave activity (dSWA), and mean firing rate (mean FR). Points indicate channels grouped by animal (left to right), but boxplots reflect channels from all animals treated as one population. (**E**) An example scatter plot of the correlation between the change in median SWA from one NREM episode to the next and the mean firing rate during the intervening period of wakefulness. This channel is representative because it has the median correlation coefficient of all channels.

The online version of this article includes the following source data for figure 1:

Source data 1. Slow wave activity, firing rate and vigilance state time series data.

Achermann, 2011; ***Guillaumin et al., 2018***). To explore whether spike firing rates might account for some of the variation in the rate of increase of Process S, we correlated the change in LFP SWA from one NREM sleep episode to the next, when separated by wakefulness lasting at least 5 min, with the mean spike firing rate during this intervening wake period, and with the duration of that wake period. Correlation coefficients were obtained separately for each recording channel, and pooled across animals. As expected, we obtained large positive correlation coefficients between the duration of a period of wakefulness and the change in LFP SWA in all channels (mean = 0.66, sd = 0.13; ***Figure 1D***). Importantly however, the change in LFP SWA was on average also positively correlated with the firing rate (mean = 0.27, sd = 0.30; ***Figure 1D,E***), meaning that, generally, a higher firing rate during waking was associated with a larger increase in SWA in subsequent NREM sleep. Interestingly, these phenomena were not independent, as a positive correlation was also found between wake episode duration and firing rate (mean = 0.35, sd = 0.33; ***Figure 1D***). These results further support the possibility that neuronal activity is associated with Process S dynamics. To test this hypothesis, we next turned to a quantitative modelling approach.

Process S dynamics can be described as a function of temporally and spatially integrated local neuronal activity

We first sought to determine whether a model expressing Process S dynamics solely as a function of local multi-unit firing rates might describe the levels of sleep SWA in the corresponding LFP with comparable accuracy to the classical model which is dependent on vigilance states defined at the global level (***Figure 2***). The classical Process S model was used as a starting point for the development of a novel firing-rate-dependent alternative. To do this, the equations of the classical model were adapted in two ways. Firstly, an instantaneous firing rate threshold ($\boldsymbol{F_\theta}$) was introduced as a new model parameter to replace the wake vs. sleep criterion, assuming an increase in Process S when the threshold is exceeded and a decrease when firing is below. Conceptually, this firing rate threshold resembles a set point: a target firing rate at which the dynamics are stable. Secondly, we assumed that the rate of change of Process S is proportional to the difference between firing rate and this threshold. Introducing this change to the equations ensures that the rate of change of $\boldsymbol{S}$ is equal to zero exactly at the set point, and a continuous function of firing rate around this value. This version of the model is later abbreviated as Fr-SWA. The equations are (***Figure 3A***):

$$F(t)>F_\theta: \quad \frac{dS}{dt} = \alpha(S_{max} - S(t))(F(t) - F_\theta)$$

$$F(t)<F_\theta: \quad \frac{dS}{dt} = -\beta(S(t) - S_{min})(F_\theta - F(t))$$

$$F(t) = F_\theta: \quad \frac{dS}{dt} = 0$$

We applied this novel model, alongside the classical model, to describe SWA dynamics at the LFP level, by finding parameter values that would minimise the difference between empirical SWA and modelled Process S. The two models were fit to the SWA from each LFP channel separately, using the multi-unit firing rate from the same channel for the firing-rate-dependent model. The

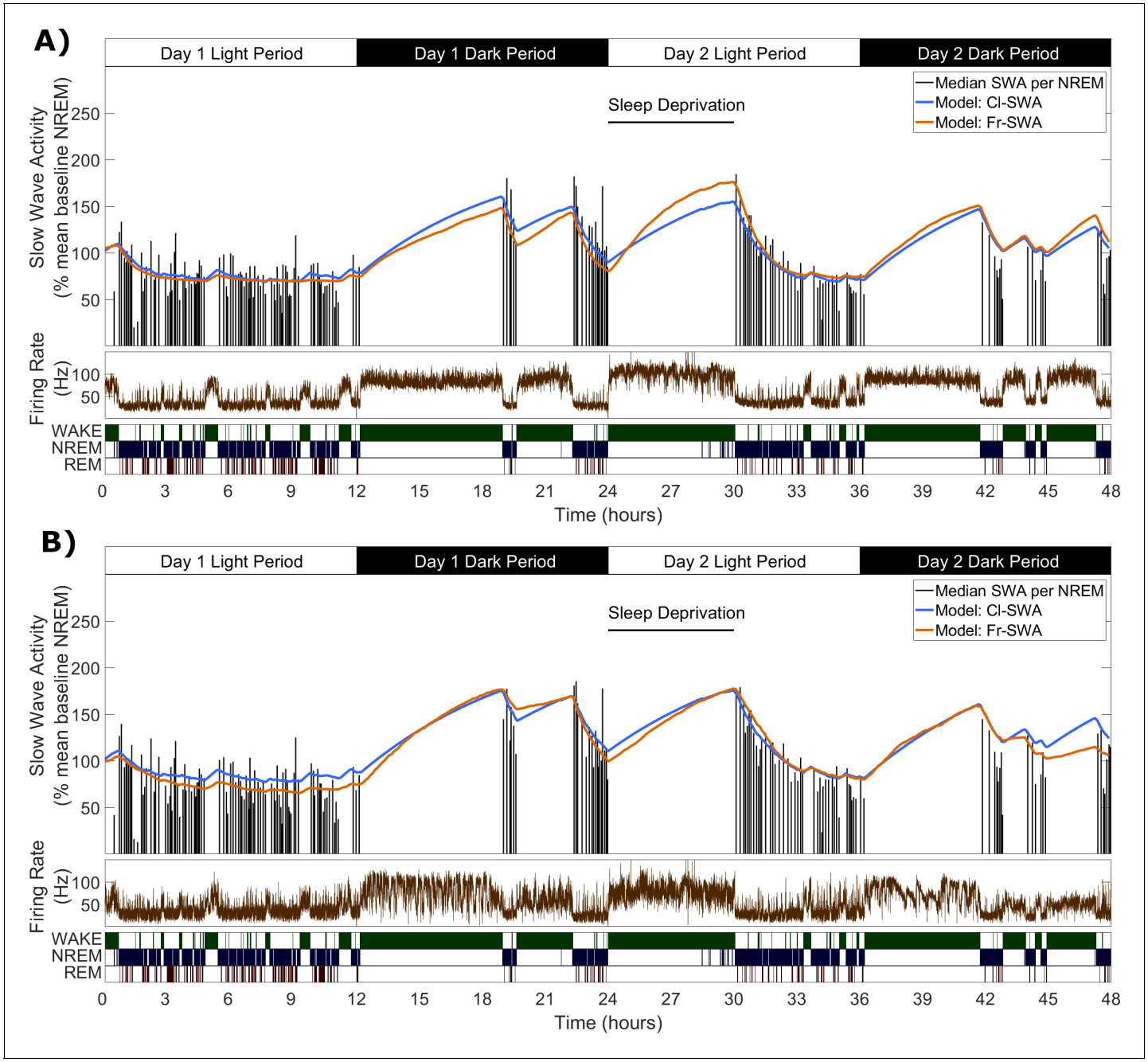

Figure 2. Slow wave activity dynamics at the LFP level can be modelled using multi-unit spiking information. (**A**) An example from one representative animal modelling the SWA averaged over all LFP channels, of both the classical model (blue) and novel firing-rate-based model (orange), calculated from the firing rate also averaged over all LFP channels (brown). (**B**) An example of both models applied to the SWA of a single LFP channel, which came from the same animal as used in **A**.

models were also fit to the SWA obtained by averaging the LFP (and firing rate) over the whole population of channels within the same mouse.

Figure 2 shows two examples of the fit of both models, first to SWA derived from the average LFP, and also to SWA derived from a single LFP channel (these examples are from the same animal as in ***Figure 1A***). The overall pattern of Process S dynamics was similar at both LFP and EEG recording levels and was well described by both the classic and novel firing-rate-based model. Throughout the data, this purely firing-rate-dependent model described the overall dynamics of LFP SWA during NREM sleep to a comparable accuracy as the classical model, as reflected in the median percent

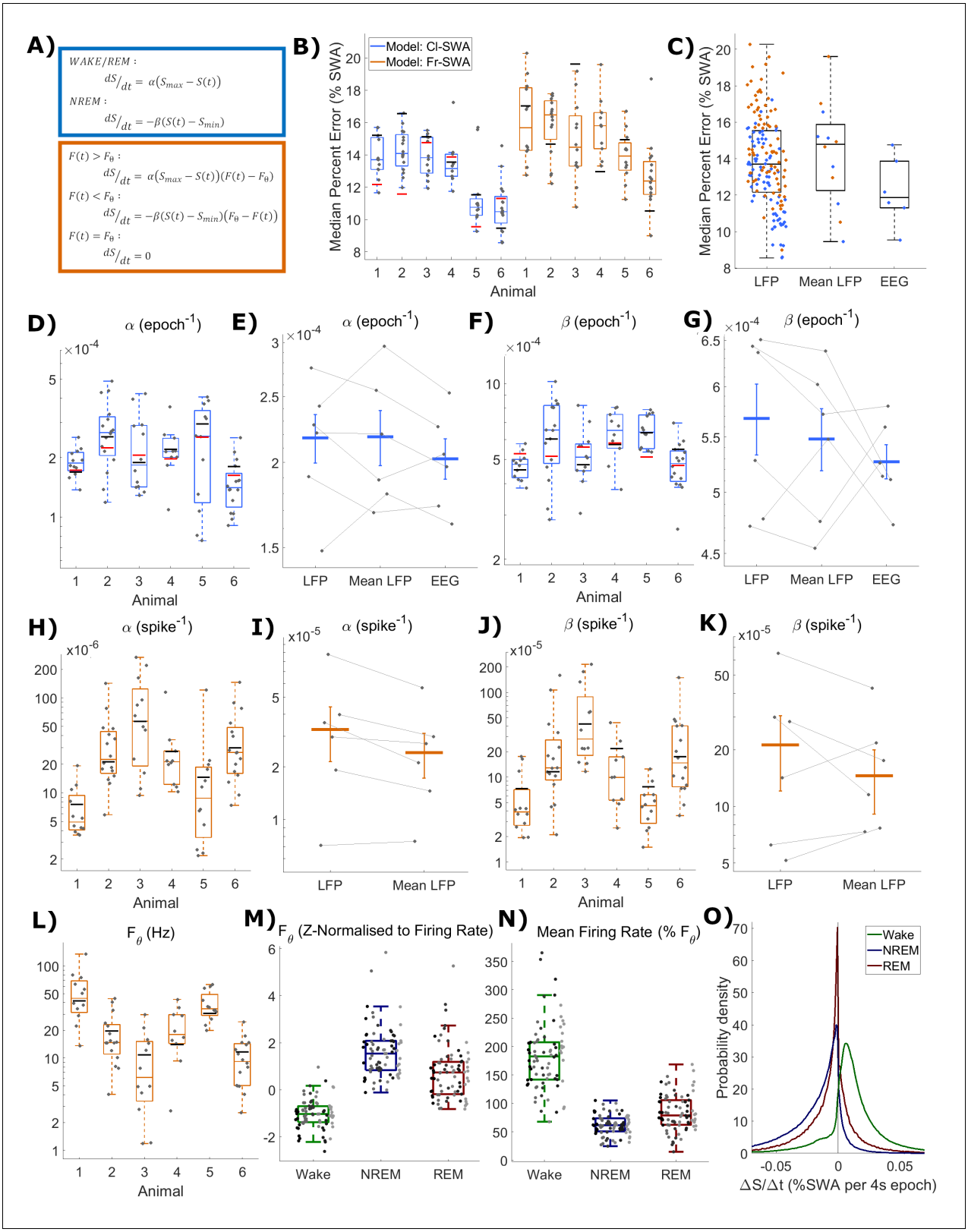

Figure 3. The fit quality and parameters for both classical and firing-rate-based models of LFP SWA. (**A**) Equations for the classic state-based model (blue) and novel firing-rate-based model (orange). (**B**) For each animal, the distribution over channels of the median absolute difference between the model and empirical SWA, expressed as a percentage of empirical SWA, for both classic and firing-rate-based models. Black lines indicate the values obtained from modelling the averaged LFP SWA and firing rate over all channels within an animal and the red lines give the parameter value obtained

Figure 3 continued on next page

Figure 3 continued

from the model applied to the frontal EEG SWA of that animal. (**C**) The same median percent error, grouped over animals and models, separately showing errors at the level of single LFP, averaged LFP and EEG. (**D–K**) The distribution (log scale) of values estimated for α and β rate parameters in the classic model (blue) and in the firing-rate-based model (orange). Parameter values are first presented with boxplots plotted separately for each animal (**D, F, H, J**), then are additionally shown grouped by level of analysis (**E, G, I, K**), including single LFP channel, mean of LFPs, or (**E** and **I** only) frontal EEG. Vertical lines indicate the standard error of the group mean and grey lines connect points derived from the same animal across groups. (**L**) The distribution of the final optimised value for the firing rate set point parameter (F_θ) of the firing-rate-based model grouped by animal. (**M**) The same values z-normalised to the distribution of firing rates within wake, NREM and REM sleep. (**N**) The distribution of mean firing rate in wake, NREM and REM sleep, expressed as a percentage of the firing rate set point parameter (F_θ). Points indicate channels grouped and coloured by animal, but boxplots reflect all channels treated as one population. (**O**) The distribution of the change in Process S ($\Delta S/\Delta t$) from one 4 s time step to the next derived from the Fr-SWA model in wake, NREM sleep and REM sleep. All mice, channels and time are pooled.
The online version of this article includes the following source data and figure supplement(s) for figure 3:

Source data 1. Process S time series and parameters based on SWA for classic and novel models.
Figure supplement 1. Values for S_{max} and S_{min} parameters in Process S models derived from SWA.

error deviation between modelled and empirical SWA (***Figure 3B***). Both the model type and animal had a highly significant effect on the median percent error of the model fit to individual LFP channels, although there is no significant interaction (Model: $F_{(1,144)}$=25.9, p=1.1×10^{-6}; Animal: $F_{(5,144)}$=30.2, p=6.3×10^{-21}; Model x Animal: $F_{(5,144)}$=1.65, p=0.15; two-way ANOVA unequal groups). Errors were higher for the novel model, importantly however, the differences in fit quality due to the model type are small relative to the effect of the particular animal and channel, on which fit quality depends much more strongly (Model: η^2 = 0.079; Animal: η^2 = 0.459; Model x Animal: η^2 = 0.025; Channel (residuals): η^2 = 0.437). The errors of the model fit on the averaged LFP and on the EEG (classical model only) are also shown in ***Figure 3B***, and are more explicitly compared in ***Figure 3C***. We did not find any significant effect of the field potential level (EEG, average LFP, single LFP channels) on the model error ($F_{(2,171)}$ = 0.2, p=0.82, one-way ANOVA).

The distributions of final optimised rate parameters, α and β, are shown in ***Figure 3D–G*** for the classic model and ***Figure 3H–K*** for the firing-rate-based model. In all cases, it was observed that the optimised rate parameters for Process S derived from EEG and the mean LFP consistently fall within the range of corresponding parameters derived from single LFP channels, suggesting that Process S calculated at spatially higher levels may reflect an averaging of Processes S which exist more locally. Indeed, for both rate parameters in both models, the mean of parameter values over single-channel-derived Process S was not significantly different from the equivalent parameter values obtained from the mean LFP or EEG (Cl-SWA α: $F_{(2,10)}$ = 1.0, p=0.39; Cl-SWA β: $F_{(2,10)}$ = 0.7, p=0.51; two-way ANOVA, factors spatial level and animal; Fr-SWA α: p=0.079; Fr-SWA β: p=0.24; paired t-test). The final optimised values of the firing-rate threshold parameter, F_θ, in the activity-dependent model are shown in ***Figure 3L***, and the values of S_{max} and S_{min} in both models are shown in ***Figure 3—figure supplement 1***. Most parameters in both models were significantly different between animals, with the exception of S_{min} in the firing-rate-dependent model (Cl-SWA α: $F_{(5,77)}$ = 4.03, p=2.8×10^{-3}; Cl-SWA β: $F_{(5,77)}$ = 8.65, p=1.9×10^{-6}; Cl-SWA S_{max}: $F_{(5,77)}$ = 14.35, p=9.8×10^{-10}; Cl-SWA S_{min}: $F_{(5,77)}$ = 12.42, p=1.1×10^{-8}; Fr-SWA α: $F_{(5,77)}$ = 8.33, p=3.0×10^{-6}; Fr-SWA β: $F_{(5,77)}$ = 9.27, p=7.5×10^{-7}; Fr-SWA F_θ: $F_{(5,77)}$ = 14.3, p=1.0×10^{-9}; Fr-SWA S_{max}: $F_{(5,77)}$ = 6.64, p=3.9×10^{-5}; Fr-SWA S_{min}: $F_{(5,77)}$ = 2.16, p=0.07; one way ANOVA).

The relationship between the optimal firing set point and state specific firing rates is shown in ***Figure 3M***. Firing rate threshold was z-normalised (subtract the mean firing rate over a given state and divide by the standard deviation) separately with respect to the distribution of firing rates in wake, NREM and REM sleep. This shows, as expected, that the set point is typically below mean firing in wake (−1.0 ± 0.6; mean ± sd), well above mean firing in NREM sleep (1.6 ± 1.1), and slightly above mean firing in REM sleep (0.7 ± 1.1). These were all significantly different from zero (Wake: p=1.6×10^{-13}, NREM: p=1.9×10^{-14}, REM: p=3.4×10^{-7}, two-sided Wilcoxon signed rank test). ***Figure 3N*** further shows the state-dependent distribution of average firing rate, expressed as a percentage of the chosen firing set point parameter. Mean firing was 182 ± 57.6% of the firing rate set point during wake, 61.8 ± 17.6% during NREM sleep, and 84.2 ± 31.8% during REM sleep. Again, these distributions were all significantly different from 100% (Wake: p=6.7×10^{-14}, NREM: p=2.0×10^{-14}, REM: p=5.4×10^{-5}). Note that, in a few channels, the optimal firing rate threshold is

actually above the mean firing rate during waking. This occurs when the waking firing rate distribution overlaps substantially with the NREM sleep firing rate distribution but has a heavier tail. REM sleep, in this data, is typically associated with firing below the set point, and therefore Process S decreases, albeit at a reduced rate compared to NREM sleep (***Figure 3O***). Interestingly, there are no significant correlations between the model fit error and the threshold normalisation relative to any one vigilance state (Wake: p=0.06, r = 0.21; NREM: p=0.35, r = −0.11; REM: p=0.94, r = −0.01), suggesting that there is no clear relationship between the firing rate set point and firing rate distribution of any one particular state.

Off occupancy as a novel metric for local sleep-wake related neuronal dynamics

When considering the relationship between multi-unit firing rates and LFP slow waves, a conceptual complication arises due to the different origins of the LFP and MUA from within the same channel. While the MUA firing rate represents the activity of only a few individual neurons, factors such as volume conduction result in spatial smoothing of the LFP signal, and as such it can be influenced by the activities of neurons covering a cortical area potentially on the order of several millimetres (***Kajikawa and Schroeder, 2011***). Subthreshold currents also influence the LFP (***Reimann et al., 2013***; ***Ness et al., 2016***). This means that when a slow wave is detected in the LFP, it is not guaranteed that all local neurons contributing to the MUA are necessarily silent (***Todorova and Zugaro, 2019***). Similarly, not every long interspike interval occurs during a slow wave. An estimation of the occurrence of off periods may be obtained by combining LFP and spiking data (***Figure 4A***). Slow wave detection was performed on each LFP over the whole 48 h, including all vigilance states (0.5–6 Hz filter followed by an amplitude threshold, values shown in ***Figure 4C***). All multi-unit inter-spike intervals (ISIs) which coincide with the peak of detected slow waves were identified. The distribution of the duration of these ISIs was often (64 out of 75 channels) unambiguously bimodal (***Figure 4B***). This could be interpreted as evidence of the existence of two spiking states occurring locally during the more widespread network slow oscillation: high frequency spiking (on period) and extended silence (off period). Note that these two distributions do not simply correspond exactly to sleep vs. wake conditions, because bimodality is often evident in the distribution of slow wave coincident ISIs from NREM sleep only, or even from REM sleep only (***Figure 4B***). The distribution of slow wave coincident ISIs (over all vigilance states) was used to define an ISI duration threshold for the detection of off periods, separately for each channel. The values used for this threshold are shown in ***Figure 4D***. The average multi-unit firing rate aligned to the peak of slow waves in detected off periods reveals a clear suppression of firing, consistent with expectations (***Figure 4E***). A rebound increase in average firing is visible in this example channel immediately after the off period, as has been previously documented in some cortical neuronal populations (***Chauvette et al., 2010***). The total fraction of time each channel spends in off periods was calculated over all epochs of 4 s, and termed the 'off occupancy'. Off occupancy defined in this way is high in NREM sleep and low in both wake and REM sleep (***Figure 4F***). The existence of a non-zero frequency of local cortical off periods has been previously reported during wakefulness (***Vyazovskiy et al., 2011***; ***Vyazovskiy et al., 2014***; ***Fisher et al., 2016***), and REM sleep (***Funk et al., 2016***). The off occupancy measure displays similar temporal dynamics to LFP (and EEG) SWA over both sleep deprivation and spontaneous sleep and wake (***Figure 4G***). These results together demonstrate that the detected off periods were likely to be physiologically meaningful and that, for instance, the possible inclusion of interneurons in the MUA which may spike during off periods (***Zucca et al., 2019***) did not represent a significant problem.

Process S dynamics, defined using off periods, can be described as a function of vigilance states or neuronal firing rates

In order to investigate whether the off occupancy measure reflects Process S, we applied the classical state-based model to the time course of off occupancy, exactly as was done with single channel SWA. The classical model was applied with its equations unchanged, and is abbreviated as Cl-Off. ***Figure 5A*** shows an example of the resulting Process S time course obtained in this way with a high quality of fit. In contrast, some changes were introduced to the firing-rate-based model in order to describe off occupancy dynamics. We considered that the different dynamics above vs. below a particular firing rate set point may be due to two opponent processes simultaneously active in dynamic

Figure 4. Definition of off periods and off occupancy. (**A**) An example section of LFP (raw in grey, 0.5–6 Hz filtered in black) and simultaneous MUA spikes. During this time window, the filtered LFP crosses the amplitude threshold (265 µV for this channel, red line) five times. The MUA inter-spike interval aligned to two of these peaks exceeds the duration threshold (85 ms for this channel) and so two off periods are detected (grey boxes). ISIs aligned to the other three out of five crossings (asterisks) are too short to be considered off periods. (**B**) Histograms of multi-unit inter-spike intervals

Figure 4 continued on next page

Figure 4 continued

aligned with detected slow waves (0 = peak of slow wave) for this example channel. The four plots show, from left to right, ISIs over the whole recording and ISIs separately during wake, NREM and REM sleep only. The ISI duration threshold (red line) is selected using the histogram of all ISIs (leftmost) at the minimum between the two modes (and shown for comparison in the wake, NREM and REM sleep panels). (**C**) The distribution of LFP amplitude and (**D**) ISI duration threshold values used for definition of off periods for each channel, with boxplots plotted separately for each animal. (**E**) The mean multi-unit firing rate over a period of 1 s centred on the peak of detected slow waves, calculated over all slow waves within one example channel with a resolution of 1 ms. (**F**) Distributions of mean off occupancy (%) for all channels averaged over wake, NREM and REM sleep. Points indicate channels grouped by animal (left to right), but boxplots reflect all channels treated as one population. (**G**) Off occupancy is shown alongside EEG and LFP SWA for an example channel over 48 h. Traces represent these values calculated at 4 s resolution (light grey), in addition to the median value per NREM sleep episode, as used for model fitting (black bars). Firing rate (brown) and scored vigilance states are also shown.
The online version of this article includes the following source data for figure 4:

Source data 1. Off occupancy time series and off period detection parameters.

opposition but with differential magnitude in wake vs. NREM sleep. Specifically, we consider a Process S increasing term which is proportional to instantaneous firing rate, and a Process S decreasing term which is proportional to the time spent in off periods (off occupancy). The equation used is:

$$\frac{dS}{dt} = \alpha F(t)(S_{max} - S(t)) \; - \; \beta X(t)(S(t) - S_{min})$$

In this model (***Figure 5B***), one term drives $\boldsymbol{S}$ towards an upper asymptote ($\boldsymbol{S_{max}}$) in proportion to firing rate ($\boldsymbol{F}$), while the other drives $\boldsymbol{S}$ towards a lower asymptote ($\boldsymbol{S_{min}}$) in proportion to the off occupancy ($\boldsymbol{X}$). Again, two rate parameters $\boldsymbol{\alpha}$ and $\boldsymbol{\beta}$ are required. This model behaves similarly to previous models because firing is high in wake and low in NREM sleep, whereas off occupancy is high in NREM sleep and low in wake. This variant of the model is abbreviated as Fr-Off. ***Figure 5A*** also includes the fit from this model, demonstrating a high level of agreement between the two models and an accurate fit to the data.

The distribution of the median percent errors for the fits from both models over all animals and channels is shown in ***Figure 5C***. As before, the model type and animal has a significant effect (Model: $F_{(1,138)}$ = 8.06, p=5.2×10^{-3}; Animal: $F_{(5,138)}$ = 17.2, p=3.2×10^{-13}; Model x Animal: $F_{(5,138)}$ = 0.52, p=0.76; two-way ANOVA with unequal groups), and the classic model achieved a slightly lower median percent error. However, this effect was again very weak compared with the variation in fit quality between animals and channels (Model: η^2 = 0.034; Animal: η^2 = 0.367; Model x Animal: η^2 = 0.011; Channel (residuals): η^2 = 0.588). ***Figure 5D*** shows the distribution of values for the change in modelled Process S from one simulated time step to the next resulting from the firing-rate-based model (Fr-Off), in wake, NREM and REM sleep, pooling all animals, channels and time. Unlike in the previous firing-rate-based model, REM sleep is now typically associated with an increase in Process S. The distributions of final optimised rate parameters, α and β, are shown in ***Figure 5E–F*** for the classic model and ***Figure 5G–H*** for the firing rate and off occupancy model. Values for $\boldsymbol{S_{max}}$ and $\boldsymbol{S_{min}}$ are shown in ***Figure 5—figure supplement 1***. Most parameters in both models were different between animals (Cl-Off α: $F_{(5,74)}$ = 2.4, p=0.047; Cl-Off β: $F_{(5,74)}$ = 2.29, p=0.055; Cl-Off $\boldsymbol{S_{max}}$: $F_{(5,74)}$ = 9.49, p=6.4×10^{-7}; Cl-Off $\boldsymbol{S_{min}}$: $F_{(5,74)}$ = 16.79, p=8.0×10^{-11}; Fr-Off α: $F_{(5,74)}$ = 9.86, p=3.9×10^{-7}; Fr-Off β: $F_{(5,74)}$ = 5.14, p=4.6×10^{-4}; Fr-Off $\boldsymbol{S_{max}}$: $F_{(5,74)}$ = 10.08, p=2.8×10^{-7}; Fr-Off $\boldsymbol{S_{min}}$: $F_{(5,74)}$ = 10.25, p=2.3×10^{-7}; one way ANOVA). Notably, the weakest evidence for inter-animal differences were for α and β in the classic model.

Variation in local process S dynamics is averaged away at higher scales and is stable across conditions

Although we demonstrated that the rate parameters obtained at the local level appear to correspond closely to those obtained for 'global' EEG, the question remains how local activity-dependent Processes S might relate to the global Process S which reflects sleep-wake history. To enable the direct comparison of their time courses, each Process S was normalised in a range from zero to one, determined by the corresponding fitted values of $\boldsymbol{S_{max}}$ and $\boldsymbol{S_{min}}$. We observed that the mean over individual Processes S derived from applying activity-dependent models in single channels matches the time course of Process S derived from the EEG with the classical model. This held for both local SWA (***Figure 6A***) and off occupancy (***Figure 6B***) models. Note that the Cl-SWA model is considered

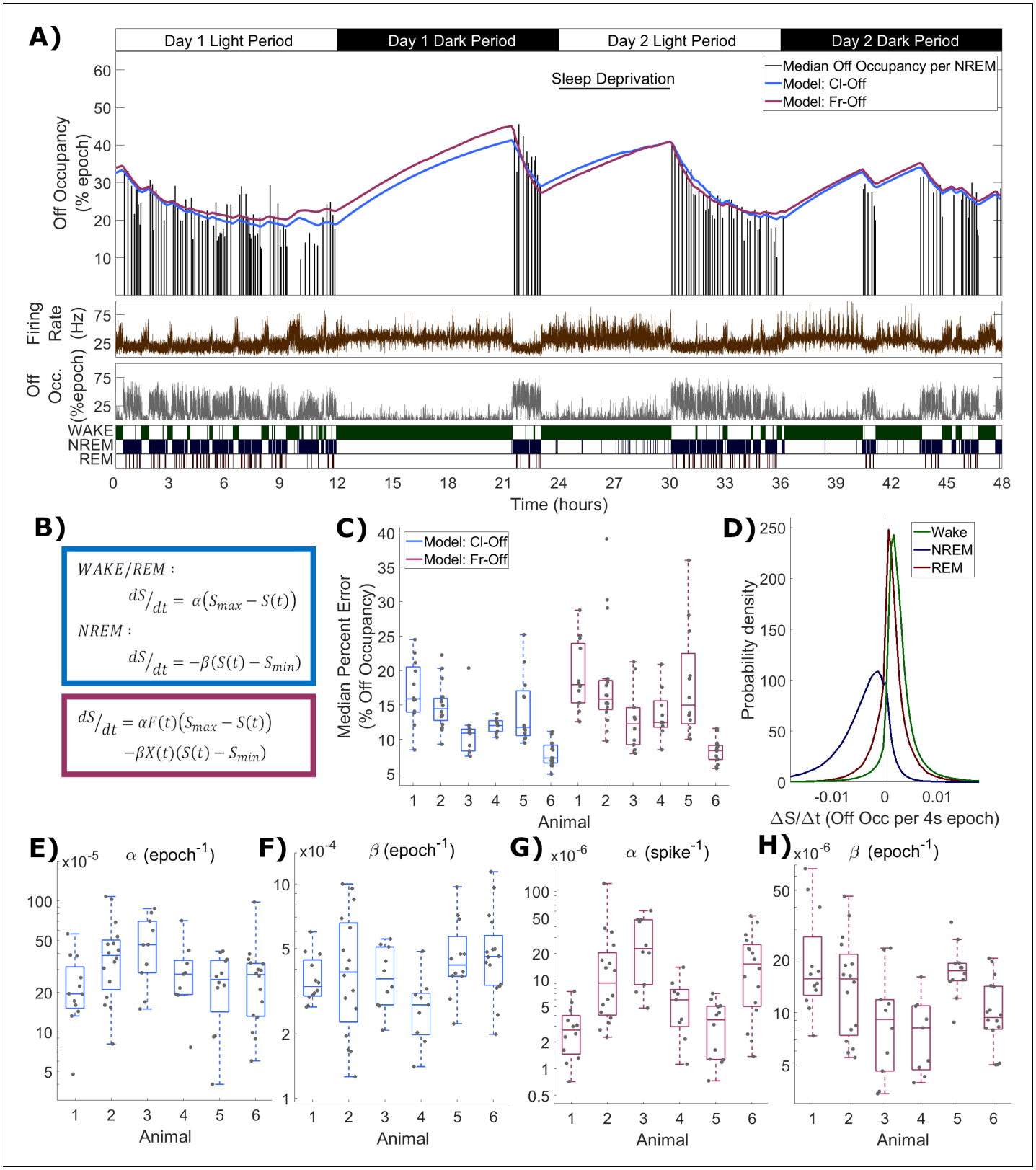

Figure 5. Process S is reflected in an LFP channel's off occupancy and its dynamics are described well by both state-based and firing-rate-based models. (**A**) An example of the novel model based on firing rates and off occupancy (purple), and the classic state-based model (blue), with optimised parameters describing the dynamics of off occupancy (median per NREM episode, black bars) over 48 h. Sleep deprivation occurred as indicated at light onset of the second day and lasted 6 h. Firing rate (brown), off occupancy (value per 4 s epoch, grey) and scored vigilance states are also shown.

Figure 5 continued on next page

Figure 5 continued

(**B**) Equations for the classic state-based model (blue) and firing-rate-and-off-occupancy-based model for off occupancy (purple). (**C**) For each animal, the distribution over channels of the median difference between the model and empirical off occupancy, expressed as a percentage of the off occupancy, for both classic and firing-rate-based models. (**D**) The distribution of values of the change in Process S ($\Delta S/\Delta t$) from one 4 s time step to the next derived from the Fr-Off model in wake, NREM sleep and REM sleep. All mice, channels and time are pooled. (**E–F**) The distribution of optimised values used for the rate parameters in the classic model and (**G-H**) the firing rate model, with boxplots plotted separately for each animal.
The online version of this article includes the following source data and figure supplement(s) for figure 5:

Source data 1. Process S time series and parameters based on off occupancy for classic and novel models.
Figure supplement 1. Values for S_{max} and S_{min} parameters in Process S models derived from off occupancy.

in both cases here, as this is the most 'global' level at which the model can be applied, and off periods are not defined for the EEG. Interestingly, over all animals the global level Process S was typically in between the average of local Processes S derived from the two activity-dependent models (***Figure 6C***). This result suggests that global Process S calculated at a higher spatial scale might reflect an averaging across a manifold of local Processes S that exist on a finer spatial level.

The modelling approaches described here all identify variability in Process S between recording channels, and indicate that a local component determines its temporal dynamics, which, in turn, is spatially integrated to give rise to the global dynamics of Process S. One important caveat that remains is that, even within the same global behavioural state, neuronal activity recorded from the same local cortical region may differ markedly between recording conditions, depending, for example, on the time of day or specific wake behaviours. Therefore, if the dynamics of global Process S represent spatial integration of local neuronal activities, it is important to determine how stable the locally-derived rate parameters are, and how sensitive our overall modelling approach is, to factors which are expected to influence local neuronal firing rates.

To address this question, we performed parameter estimation for each model separately for baseline day, when the animals are awake spontaneously for most of the dark phase, and for the day when sleep deprivation was conducted, when the animals are engaged in novel object exploration and spent time awake for an extended period of time during the light phase, when nocturnal mice are habitually asleep. Invariably, we observed that both the rate parameters and the median error were close to those derived from the whole 48 h, with parameters clustering around 100% of their original values and error differences around zero (***Figure 6—figure supplement 1***). Statistical analysis (***Figure 6—figure supplement 1***) suggested that the day, baseline or sleep deprivation, did have a significant effect on all parameters and error differences, suggesting some influence on Process S which is unaccounted for both by global sleep-wake history and cortical activity. The model type, either classical (state-based) or novel (activity-based), was generally only significant for Process S models based on SWA, not off periods. Importantly, the interaction between day and model was not significant in most cases, supporting that the activity-dependent models describe day-dependent variation in Process S generally similarly to the classical sleep-wake state model. Indeed, in the one case in which a significant interaction effect was found (β in off periods models), day-dependent differences were greater for the classical model than activity-dependent model (***Figure 6—figure supplement 1E***). The effect of animal was variably significant, although the interaction between animal and day was significant in all cases. This further suggests that variation in Process S errors may be associated with inter-individual variability arising from technical factors, such as precise location of the recording electrode, or systematic differences in the animals' behaviour, rather than due to the modelling approach.

Discussion

Here, we demonstrated that Process S dynamics can be derived entirely from multi-unit neuronal spiking activity, without reference to global sleep-wake states. A model was outlined whereby the integrated history of local multi-unit firing rates, relative to a locally-defined firing rate set point, predicted the temporal dynamics of LFP SWA. The accuracy of this model was demonstrated in data recorded from mouse frontal cortex over 48 h, including both voluntary sleep and wake, and sleep deprivation. A novel metric for Process S was then presented, termed off occupancy, which measures the fraction of time a neural population spends in off periods, defined by the coincidence of

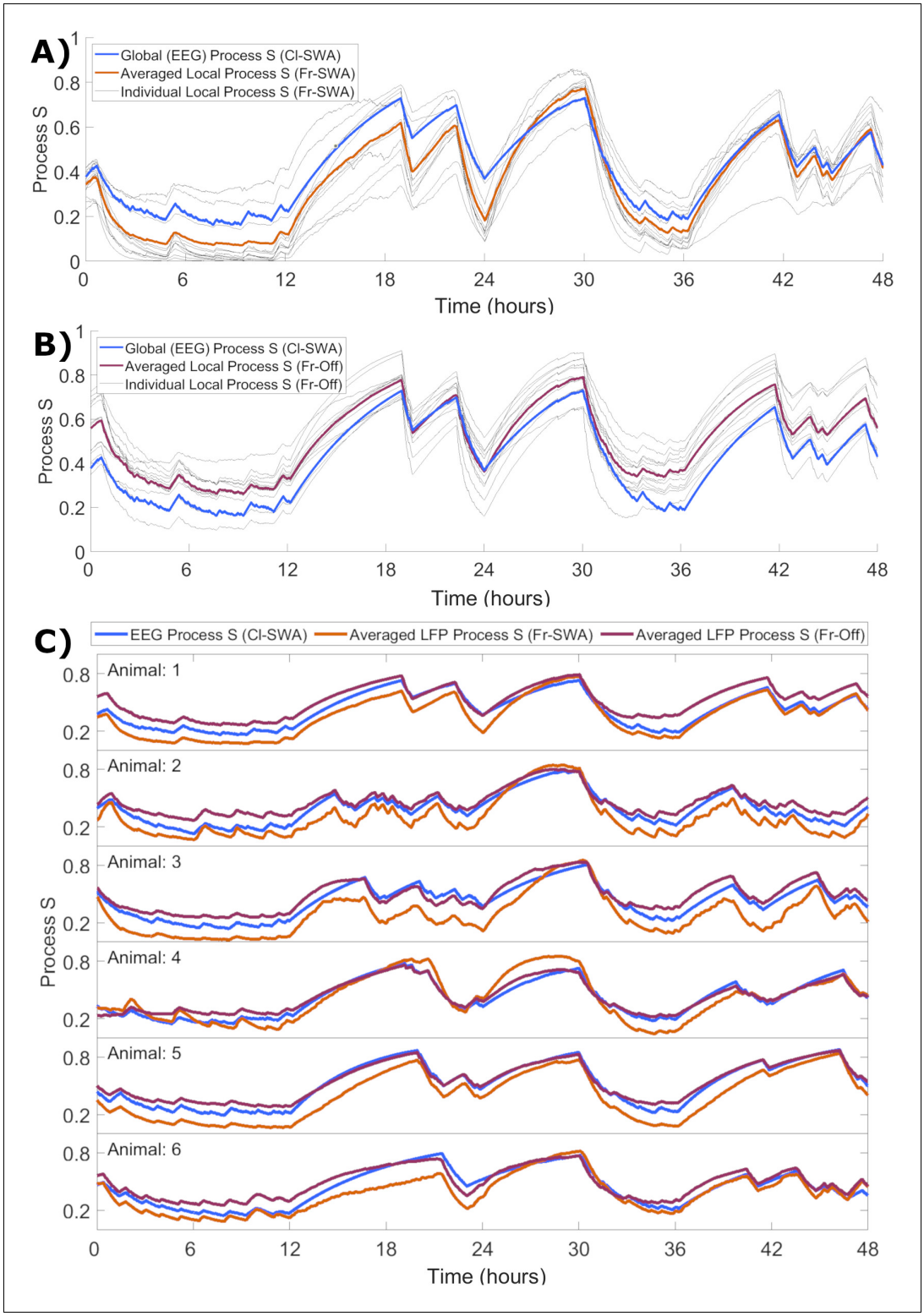

Figure 6. The time course of local activity-derived Process S averaged across channels resembles Process S derived from the EEG and sleep-wake history. (**A**) The time course of Process S shown for one representative animal using the classical EEG-based model (blue), alongside average (orange) and individual channel (grey) Processes S derived from activity-dependent models of all individual LFP channels applied to SWA. (**B**) The same, except that Process S corresponding to individual channels (grey) and their average (purple) are derived from off periods. Note that the model in blue remains Cl-SWA, as off periods cannot be derived from the EEG. (**C**) Process

Figure 6 continued on next page

Figure 6 continued

S derived from applying the Cl-SWA model to frontal EEG (blue) and the mean Process S derived from applying Fr-SWA (orange) and Fr-Off (purple) to all individual channels. The results are shown for each of the six animals analysed. In all panels, all Process S time series are normalised between 0 to 1 relative to individual S_{min} and S_{max} values for fair comparison.

The online version of this article includes the following figure supplement(s) for figure 6:

Figure supplement 1. Cross-validation of parameter estimation.

LFP slow waves and multi-unit spiking silence. The modelling approach was combined with the off occupancy metric and tested on the same data to present a quantitative framework for understanding dynamics of sleep pressure at a highly local level in terms of neural spiking and off periods. Importantly, it is concluded that Process S at the global level reflects sleep-wake history through an integration of local cortical neuronal activity levels over time and also across spatially distributed networks.

Central to this modelling perspective is the assumption that the generation of spikes by a neural network is in some way correlated with an increase in sleep pressure, and that this manifests in the subsequent expression of slow waves and off periods, reflecting Process S. The energetic cost of spiking is high (***Attwell and Laughlin, 2001***), the regulation of a neuron's firing rate set point is linked to cellular energetics (***Styr et al., 2019***; ***Vergara et al., 2019***), and neurons are susceptible to cellular stresses that can result from sustained metabolic load, such as oxidative stress (***Wang and Michaelis, 2010***; ***Cobley et al., 2018***; ***Kempf et al., 2019***; ***Cirelli et al., 2006***). Furthermore, spiking activity may be mechanistically associated with synaptic plasticity, and it was suggested that firing rates are an important determinant of overall changes in synaptic strength, with higher spiking leading to greater changes (***Graupner et al., 2016***; ***Lappalainen et al., 2019***). Compensatory processes exist within neurons to oppose cellular stress and related homeostatic challenges (***Kültz, 2005***) and off periods could provide the opportunity for neurons to prioritise such processes, therefore mediating the restorative benefits of sleep (***Vyazovskiy and Harris, 2013***). Similarly, off periods are associated with distinct synaptic plasticity rules (***González-Rueda et al., 2018***), and so their prevalence and patterning is likely also related to whatever regulation of synaptic strength occurs during sleep (***Tononi and Cirelli, 2014***; ***Timofeev and Chauvette, 2017***; ***Seibt and Frank, 2019***).

According to this view of sleep homeostasis, in principle, regulation can occur entirely at the local level, within cortical networks or perhaps even within single neurons. Indeed, this is reflected in our results through the differences between channels both with respect to the accuracy of the model and in the values of optimised parameters. Why then is global sleep preferred over a hypothetical state including asynchronous local off periods, which presumably could be used to sustain longer periods of behavioural wakefulness? It has been argued previously that it is ecologically optimal to synchronise off periods and undergo dedicated periods of total behavioural shutdown, because local off periods during waking impair behaviour (***Vyazovskiy et al., 2011***; ***Rattenborg et al., 2012***). Mechanistically, the occurrence of off periods might be obstructed by strong synaptic coupling and shared neuromodulatory tone. Indeed, it has been observed that the degree of coupling between an individual neuron's firing and the population firing rate, is variable between cells but characteristic to an individual neuron and likely reflects total synaptic strength with its neighbours (***Okun et al., 2015***). Some neurons may therefore be less able to express asynchronous off periods than others.

The preference for global sleep, despite its fundamentally local mechanisms, may be evidence that sleep homeostasis ultimately does not serve a single specific local function. Instead, the recent history of neuronal activity levels may regulate the local tendency to generate a signal (reflected in Process S) which is integrated over larger neuronal populations through intrinsic network mechanisms in order to produce a global sleep propensity signal that estimates the total time spent awake with great accuracy. This mechanism would enable the brain to enforce a daily quota of sleep, which could have many benefits at the physiological and ecological level, rather than to initiate sleep in response to the homeostatic need of one specific regulated variable (***Vyazovskiy, 2015***). Importantly, in this mechanism, the variables which change as a function of time spent awake or asleep do not themselves need to be directly regulated by sleep. Conversely, variables which remain stable during continuous wake or sleep could still make essential contributions to the time-keeping

mechanism. Note that this property is present in our model, since the levels of neural activity themselves are not directly proportional to the levels of Process S. The approximately equivalent overall accuracy of both firing-rate-based and vigilance-state-based models supports this possibility, as does the evidence that homeostatically regulated cellular variables can actually be stable during extended wakefulness, and that maintenance processes in sleep may be ultimately prophylactic (**Vyazovskiy and Harris, 2013**). In order to maximise the efficiency of global sleep, single neuronal activities may be modulated such that sleep pressure accumulates, on average, as uniformly as possible. This is consistent with recent reports that sleep regulates the population level firing rate distribution (**Watson et al., 2016**; **Levenstein et al., 2017**; **Miyawaki et al., 2019**) and could account for sleep's link with synaptic and firing rate homeostasis, reconciling the local origins of sleep pressure accumulation with the global level of its dissipation.

Here, spike firing rate is used to represent the level of neural activity because it is convenient to record, locally variable, and directly linked to neuronal functionality. However, no strong claim is made that firing rates are necessarily causally responsible for the accumulation of sleep pressure. Indeed, it would likely be possible to obtain a reasonable quantitative account of sleep homeostasis using any physiological variable (or set of variables) that are consistently higher in either the wake or sleep state. For example, a model assuming that Process S increases in proportion to local cortical temperature, which, in laboratory rodents, drops by ~2˚C when falling asleep (**Franken et al., 1991b**; **Tobler et al., 1997**) and which has been mechanistically implicated in sleep regulation (**Hoekstra et al., 2019**), might also provide a plausible description of Process S dynamics. However, our results demonstrate that firing rates are a useful measurable correlate of the processes that directly underpin Process S, and therefore firing rate variance resulting from differences in experience and behaviour may well account for the variance in Process S accumulation in normal individuals, between waking periods and between cortical regions.

It should be noted that the firing-rate-based models used here typically slightly under-perform, relative to the classic model, in terms of minimising the error between simulation and empirical data. A limit on the accuracy of the model might be expected, related to technical restrictions rather than conceptual ones. In this approach, neuronal activity was considered at the multi-unit level, which comprises only a few randomly sampled nearby neurons. Certainly, individual neurons vary in their firing properties (**Watson et al., 2016**) and grouping these as a single measure of local network activity is somewhat arbitrary. However, since it remains possible that firing rate homeostasis acts on the population level (**Levenstein et al., 2017**) and also that there exist substantial local spatial correlations in cortical spiking (**Okun et al., 2015**), this choice is justifiable. Therefore, it may be significant that local Process S reflects global sleep-wake history more closely than the history of local activity, supporting the idea of a spatial integration of Process S. It remains possible that these models might be applicable to firing derived from well isolated single units, although a reduction in fit quality would be predicted, owing to the proposed intrinsic spatial integration of Process S.

A direct experimental test of the conclusion that global Process S derives from a spatial and temporal integration of local neuronal activities would require neuronal activity to be recorded and manipulated simultaneously across many brain areas, including cortical and subcortical regions. A recent study, which locally activated a specific cortical area during sleep with optogenetics, did not find an increase in SWA or off periods in subsequent NREM sleep (**Rodriguez et al., 2016**). The failure of such a localised manipulation of activity to alter measurable Process S is consistent with our conclusion of spatial integration, which implies that local deviations would indeed tend to be averaged away. More global manipulations of neuronal activity, using a pharmacological approach, unfortunately come with other interpretative difficulties. For example, another study found that systemic atropine administered during behavioural wakefulness produces slow wave activity and reduces neuronal activity, yet increases the duration of subsequent NREM sleep (**Qiu et al., 2015**). While this was interpreted as evidence that spiking activity is not related to sleep pressure accumulation, crucially, the direct effects of atropine on Process S and the functional significance of the resulting induced slow oscillation are unclear. Manipulations at an intermediate scale, for example which consistently perturbed a whole cortical region, might be effective and could, in theory, exert effects beyond simple local compensatory responses, impacting also global sleep-wake states. This might not be easy to achieve methodologically, as existing approaches are often not sufficiently selective and may lead to unspecific compensatory effects.

It is reasonable to assume that sleep homeostasis unfolds over multiple time scales and that Process S as defined by these models describes a relatively fast one, approaching its upper asymptote after continuous wakefulness on a time scale of hours. The inclusion of processes acting over longer or shorter time scales might explain discrepancies in all these models, however, the challenge remains to identify what these could be. Brain processes which unfold over multiple scales have previously been explained using the theory of criticality, which implies self-similarity across many spatial and temporal scales. It is possible that the magnitude of the deviation of cortical activity from the critical point might reflect the levels of Process S, as has been previously suggested (**Pearlmutter and Houghton, 2009**; **Meisel et al., 2013**). Alternatively, since waking dynamics may be slightly subcritical, and NREM sleep slightly supercritical (**Priesemann et al., 2013**), the deviation from criticality could, in principle, contribute to the dynamics of Process S. Crucially, it remains unclear to what extent criticality and sleep homeostasis are linked and by what mechanisms, although firing rate homeostasis is likely also relevant (**Hsu and Beggs, 2006**). Addressing this question would require datasets comprising a large number of widely spatially distributed recording sites, and well isolated individual neurons.

The role of REM sleep in Process S dynamics has not been explicitly addressed or considered in the construction of these models. Depending on the model variant, REM sleep is associated either with a small increase or small decrease in Process S, because firing rates are low in REM sleep (closer to NREM sleep than waking) and yet off period occupancy is also low (closer to wake levels than NREM sleep). It is possible that REM sleep might represent a homeostatically neutral state, in which the level of Process S changes minimally, or not at all (**Vyazovskiy and Delogu, 2014**). Another important factor which remains unaddressed is the influence of the circadian rhythm on Process S and also on neuronal activity. It may be possible, for example, that the time-keeping mechanism derives information also from circadian signals, possibly running faster or slower at different phases of the light-dark cycle or that the neuronal firing rate set-point experiences circadian regulation.

In summary, our data suggest that Process S is reflected at multiple scales in the brain, from EEG and LFP slow wave activity to the occurrence of local multi-unit off periods. Its dynamics across all scales can be described quantitatively using information derived only from local neuronal activity with comparable accuracy to the classical model of Process S which depends on global sleep-wake history. We postulate that, despite its local origins, Process S may be integrated across networks for the purpose of tracking time spent awake and used to enforce a daily quota of global sleep, rather than serving the regulation of specific physiological variables.

Materials and methods

Animals, surgery and husbandry

Chronic electrophysiological recordings from six male adult (4.8–5.7 months old, mean 5.2 months) C57BL/6J mice were analysed here. This data set is a subset of that used in a previous study (**McKillop et al., 2018**). The animals were surgically implanted with electrodes for the continuous recording of electroencephalogram (EEG), electromyogram (EMG) and cortical neuronal activity. EEG screw electrodes (Fine Science Tools) were inserted into the skull above the frontal cortex (primary motor area: anteroposterior 2 mm, mediolateral 2 mm) and occipital cortex (primary visual area: anteroposterior 3.5 mm, mediolateral 2.5 mm). Additional screw electrodes were placed contralateral to the occipital screw and above the cerebellum to serve as the ground and reference electrodes, respectively. A pair of stainless steel wires were inserted into the nuchal muscle for the recording of EMG. A polyimide-insulated tungsten microwire array (Tucker-Davis Technologies) was implanted through a craniotomy window into the frontal cortex (primary motor area: anteroposterior 2 mm, mediolateral −2 mm), contralateral to the EEG screw. The array comprised 16 wire channels of 33 µm diameter, arranged in 2 rows of 8, with columnar separation of 250 µm, row separation of 375 µm and tip angle of 45 degrees. One row of wires was 250 µm longer than the other to account for cortical curvature. A silicone gel (KwikSil, World Precision Instruments) was used to seal the craniotomy, and dental acrylic cement used to stabilise all the implanted electrodes. Surgeries were performed under isoflurane anaesthesia (4% induction, 1–2% maintenance). Analgesics were given immediately before surgery (1–2 mg/kg metacam and 0.08 mg/kg vetergesic, subcutaneous injection) and for at least 3 days during recovery following surgery (1–2 mg/kg metacam, oral). In

addition, an immunosuppressant (0.2 mg/kg dexamethasone) was given the day before surgery, immediately before surgery and during recovery for at least 2 days. Animal wellbeing was closely monitored during recovery until a stable return to baseline was observed. All procedures were performed under a UK Home Office Project License and conformed to the Animal (Scientific Procedures) Act 1986.

Mice were housed individually following surgery. Two weeks after surgery, mice were transferred, still individually, to custom made Plexiglas cages (20.3×32×35 cm), containing a running wheel (Campden Instruments), which were placed within ventilated sound-attenuated Faraday chambers (Campden Instruments). The animals were exposed to a standard 12 h - 12 h light dark cycle, with food and water available ad libitum. Mice were allowed to habituate to the recording chamber and to attachment of the recording cables for a minimum of three days.

Experimental design

All the data analysed here were collected over two days. The first day served as a baseline, while the animals were completely undisturbed. A sleep deprivation protocol was enforced at light onset on the second day, immediately after the baseline day, and lasted 6 h. Sleep deprivation was performed using the well-established gentle handling procedure (***McKillop et al., 2018***). During this period, experimenters constantly monitored both the behaviour and ongoing neurophysiological recordings of the mice. As soon as any animal showed signs of sleepiness (such as immobility, or slow waves in the EEG), novel objects were introduced to the cage (such as cardboard, colourful plastic and tissue paper) in order to encourage wakefulness. During the sleep deprivation period of 6 h, these mice slept 6.1 ± 2.9 min (mean ± sd) only.

Data collection and pre-processing

Data acquisition was performed using a Multichannel Neurophysiology Recording System (Tucker Davis Technologies). EEG, EMG and microwire array LFP signals were filtered (0.1–100 Hz), amplified (PZ5 NeuroDigitizer preamplifier, TDT) and stored locally (256.9 Hz sampling rate). Matlab scripts were used for signal conversion and data pre-processing. The LFP, EMG and EEG signals were filtered again offline between 0.5–100 Hz (4th order Type II Chebyshev filter) and resampled at 256 Hz.

Extracellular multi-unit spiking was additionally obtained from each microwire array channel, recorded at 25 kHz and filtered 300 Hz – 5 kHz. An amplitude threshold (at least two standard deviations, minimum −25 μV) was used to identify putative spikes. Individual spikes were saved as a voltage waveform comprising 46 data samples (0.48 ms before to 1.36 ms after threshold crossing) plus a time stamp of occurrence. Spiking activity from each channel was cleaned offline for artefacts using the Matlab spike sorting software Wave_clus (***Quiroga et al., 2004***). All putative single unit clusters identified by the algorithm from the same channel were merged, excluding only noise spikes. MUA firing rate for each channel was calculated in epochs of 4 s and expressed in Hz.

Vigilance states were scored manually by visual inspection at a resolution of 4 s (using the software SleepSign, Kissei Comtec). Vigilance states were classified as waking (low amplitude but high frequency EEG with high or phasic EMG activity), NREM sleep (presence of EEG slow waves, a signal of a high amplitude and low frequency, and a low level of EMG activity) or REM sleep (low amplitude, high frequency EEG, and low EMG). All individual recording channels were manually visually examined in order to identify low quality signals which were characterised by poor signal to noise ratio, frequent artefacts, unsystematic rapid changes in firing rates, or major drifts in spike number across the recording period, that could not be related to the ongoing state. Such issues were considered to arise from technical issues and phenomena which were not physiological and these channels were excluded. For this analysis, over the six mice, a total of 78 out of 96 channels could be analysed (minimum of 10 out of 16 from each mouse). For the off occupancy models described below, 75 out of 96 channels were used; a further three channels were excluded because multi-unit firing rates, while stable, were too low to yield a reasonable estimate of the occurrence of off periods. Such a success rate is typical for electrophysiological studies where chronic in vivo recording of neuronal activity is performed in freely behaving animals across many days (***Fisher et al., 2016***; ***McKillop et al., 2018***).

Slow wave activity

Each EEG and LFP signal was processed to extract a measure of the slow wave activity (SWA). Signal segments were extracted within windows of 4 s duration and 1 s spacing (giving 3 s overlap), and Hann tapered. A Fourier transform was applied to each signal segment and the mean power in the slow wave range (frequencies from 0.5 to 4 Hz) was calculated. This measure was smoothed by finding the median over five temporally adjacent overlapping segments, yielding a SWA measurement for each sequential epoch of 4 s. For normalisation within each channel, SWA values were then expressed as a percentage of the mean SWA calculated over all artefact-free epochs scored as NREM sleep in the baseline 24 h. The median value of the SWA during each continuous NREM sleep episode served as an estimate of Process S. NREM sleep episodes shorter than 1 min (15 epochs) were excluded, as in a previous study modelling Process S in mice (***Guillaumin et al., 2018***). Brief awakenings (short arousals accompanied by movement, lasting <20 s) were excluded from analysis but were not considered to be the ending of a NREM sleep episode.

Off period detection and definition of 'off occupancy'

One aim of this study was to develop measures of Process S independent of the EEG, and so we focused on off periods, which are the neuronal counterpart of slow waves. Off periods refer to brief interruptions of spiking activity which occur synchronously across many recording sites, last approximately 70–100 ms (***Vyazovskiy et al., 2009***), and are coincident with the positive deflection of LFP slow waves (***McKillop et al., 2018***). Off periods are difficult to define objectively in extracellular recordings. In these studies, off periods were detected by pooling spikes over all channels and identifying inter-spike intervals (ISIs) that exceed a threshold duration. However, pooling spikes removes the ability to compare local differences, and an off period will go undetected if it does not involve all channels. To overcome this limitation, off periods were defined separately for each channel by looking at the co-occurrence of local slow waves and spiking silence.

There is no universally accepted method for slow wave detection, and a recent comparison suggests that a simple amplitude-threshold-based approach, while in theory adequate, may underperform due to channel differences in overall LFP amplitude and large amplitude fluctuations of higher frequencies (***Bukhtiyarova et al., 2019***). For this reason, the LFP was first filtered from 0.5 to 6 Hz (4th order Butterworth filter), and a threshold defined individually for each channel, using the median plus one median absolute deviation of the peak amplitude of all positive half waves (including all vigilance states, but excluding epochs with artefacts). All positive half waves with peak amplitude above threshold were then considered to be slow waves.

Next, for each LFP slow wave, the multi-unit spike preceding and following the slow wave peak was identified and the corresponding ISI determined. The distribution of these ISIs which coincide with slow waves was often (in 64 out of 75 channels) unambiguously bimodal, allowing the threshold to be selected at the local minimum between these two modes. When there was no evidence of bimodality a value of 120 ms was chosen, corresponding to the maximum value selected for the other channels. All inter-spike intervals aligned to slow wave peaks with a duration exceeding the threshold were considered off periods. Finally, the metric termed off occupancy was defined, for each epoch of 4 s, as the percentage of time spent in a detected off period during that epoch. Just as with SWA (see above), the median value of off occupancy over NREM sleep episodes was used to represent the level of Process S.

Model fitting and parameter optimisation

Three theoretical models were used to describe the time course of Process S (see Results). The model differential equations were solved using a discrete time approximation, iteratively updating the value of modelled Process S in time steps of 4 s (Euler method). The fitting of various models to a particular channel of data is equivalent to finding the optimal choice of parameters to achieve the closest match between simulation and empirical SWA/off occupancy. In all models, the initial value of Process S was included as an additional free parameter. The selection of parameter values for model fitting was achieved using a semi-automated approach. First, an algorithmic methodology was established, which depends primarily on the definition of an error metric to assess fit quality between modelled Process S and empirical data. For each animal, NREM sleep episodes were identified with a duration of at least 1 min. For each NREM sleep episode (***n = 1:N***), the median empirical

SWA/off occupancy (X_n), and similarly the median modelled value of Process S (S_n), were computed. The error metric (E) is defined as the sum of absolute differences between model and data, weighted by the relative episode duration (w_n). This weight was defined as the absolute duration (d_n) of the NREM sleep episode, normalised by the total duration of all episodes.

$$E = \sum_{n=1:N} w_n . |X_n - S_n|$$

$$w_n = d_n / \sum_{i=1:N} d_i$$

Algorithmic parameter optimisation was performed separately for each channel, aiming to minimise this error metric. This was achieved using the Matlab function *fminsearch*, which uses the Nelder-Mead simplex algorithm (**Lagarias et al., 1998**). Many parameter combinations produce very similar dynamics, and many possible optimal (or near-optimal) parameter regimes exist, therefore algorithmic optimisation is sensitive to initial values. For this reason, initial values for the parameters were first set manually, aided with the use of a custom-made Matlab graphical user interface. Manually selected values were then fed into the algorithmic optimisation. Final parameter values were visually inspected to ensure that this optimisation produced an improvement of fit. The source code for this interface, along with key functions for calculating slow wave activity and off periods and for algorithmically optimising model fit, are included as supplementary files.

The final fit quality of a model to the data was expressed as the median percent error (E^*). This is calculated by finding the absolute difference between median empirical (X_n) and simulated (S_n) SWA/off occupancy for each NREM sleep episode, expressed as a percentage of the empirical SWA/off occupancy in that episode. E^* is then defined as the median over all NREM sleep episodes of these difference values. This alternative error metric is used for presentation of results because it has more comprehensible units (percentage of empirical SWA/off occupancy) compared to the error metric, with arbitrary units.

$$E^* = \underset{n=1:N}{\text{median}} \left[\frac{|X_n - S_n|}{X_n} \cdot 100\% \right]$$

In order to cross-validate the parameter selection, the automatic parameter optimisation approach was applied again to only the rate parameters (α and β, see Results) separately over halves of the data corresponding to the baseline day and sleep deprivation day. For this, the other parameters were left unchanged from the initial semi-automated approach, since the algorithmic optimisation may perform poorly with high dimensionality. The resulting α and β parameters and associated model errors (median percent errors, E^*, calculated over the whole 48 h) were compared to those of the original parameter set.

Statistical analyses

The correlation between wake duration, wake firing rates and changes in SWA was calculated separately for each LFP channel. We first identified episodes of NREM sleep of at least 1 min duration (exactly as for modelling) and obtained the median SWA in each episode. We then identified which intervening time periods, between two NREM episodes, comprised at least 80% wake and lasted at least 5 min. We then calculated Pearson correlation coefficients between the duration of these wake periods, the mean multi-unit firing rate during these periods, and the change in median SWA from the preceding to the following NREM sleep episode.

Analysis of variance was performed to explore factors influencing model parameters and fit quality using the Matlab functions *anova1* (one-way) and *anovan* (two-way with unequal group size). For the rate parameters, ANOVA was calculated after applying a log transform. The effect size (η^2) is calculated for a factor as its sum of squares divided by the total sum of squares in the ANOVA and reflects the fraction of the variance accounted for by that factor.

To summarise the results in figures, boxplots were included alongside individual data points. These indicate the median, 25th and 75th percentiles, with whiskers extending to the most extreme value which falls within 150% of the interquartile range of the box. For these plots, results from

individual channels were typically pooled across animals. In some cases, where indicated, channels from the same animal were presented as separate populations.

Acknowledgements

BBSRC (BB/K011847/1, BB/M011224/1), MRC (MR/L003635/1), Wellcome Trust (098461/Z/12/Z), John Fell OUP Research Fund (131/032).

Additional information

Funding

Funder	Grant reference number	Author
Biotechnology and Biological Sciences Research Council	BB/K011847/1	Laura E McKillop
Biotechnology and Biological Sciences Research Council	BB/M011224/1	Christopher W Thomas
Wellcome	098461/Z/12/Z	Vladyslav V Vyazovskiy
Medical Research Council	MR/L003635/1	Vladyslav V Vyazovskiy
John Fell Fund, University of Oxford	131/032	Vladyslav V Vyazovskiy

The funders had no role in study design, data collection and interpretation, or the decision to submit the work for publication.

Author contributions

Christopher W Thomas, Conceptualization, Data curation, Software, Formal analysis, Investigation, Visualization, Methodology, Writing - original draft, Writing - review and editing; Mathilde CC Guillaumin, Conceptualization, Formal analysis, Methodology, Writing - review and editing; Laura E McKillop, Resources, Investigation, Methodology, Writing - review and editing; Peter Achermann, Conceptualization, Methodology, Writing - review and editing; Vladyslav V Vyazovskiy, Conceptualization, Supervision, Funding acquisition, Methodology, Project administration, Writing - review and editing

Author ORCIDs

Christopher W Thomas https://orcid.org/0000-0001-5371-7257
Mathilde CC Guillaumin https://orcid.org/0000-0002-8611-3852
Laura E McKillop http://orcid.org/0000-0003-3085-1175
Peter Achermann http://orcid.org/0000-0002-0208-3511
Vladyslav V Vyazovskiy https://orcid.org/0000-0002-4336-6681

Ethics

Animal experimentation: All procedures were performed under a UK Home Office Project License (P828B64BC) and conformed to guildelines set by the University of Oxford Biomedical Sciences Veterinary Services and the Animal (Scientific Procedures) Act 1986.

Decision letter and Author response

Decision letter https://doi.org/10.7554/eLife.54148.sa1
Author response https://doi.org/10.7554/eLife.54148.sa2

Additional files

Supplementary files

- Source code 1. Process S model parameter optimisation code.

- Transparent reporting form

Data availability

Data analysed during this study are included in the manuscript and supporting files. Source data files have been provided for Figures 1, 3, 4 and 5.

References

Achermann P, Dijk DJ, Brunner DP, Borbély AA. 1993. A model of human sleep homeostasis based on EEG slow-wave activity: quantitative comparison of data and simulations. *Brain Research Bulletin* **31**:97–113. DOI: https://doi.org/10.1016/0361-9230(93)90016-5, PMID: 8453498

Attwell D, Laughlin SB. 2001. An energy budget for signaling in the grey matter of the brain. *Journal of Cerebral Blood Flow & Metabolism* **21**:1133–1145. DOI: https://doi.org/10.1097/00004647-200110000-00001, PMID: 11598490

Bellesi M, Bushey D, Chini M, Tononi G, Cirelli C. 2016. Contribution of sleep to the repair of neuronal DNA double-strand breaks: evidence from flies and mice. *Scientific Reports* **6**:36804. DOI: https://doi.org/10.1038/srep36804, PMID: 27830758

Borbély AA. 1982. A two process model of sleep regulation. *Human Neurobiology* **1**:195–204. PMID: 7185792

Bukhtiyarova O, Soltani S, Chauvette S, Timofeev I. 2019. Slow wave detection in sleeping mice: comparison of traditional and machine learning methods. *Journal of Neuroscience Methods* **316**:35–45. DOI: https://doi.org/10.1016/j.jneumeth.2018.08.016, PMID: 30125590

Buzsáki G, Anastassiou CA, Koch C. 2012. The origin of extracellular fields and currents–EEG, ECoG, LFP and spikes. *Nature Reviews Neuroscience* **13**:407–420. DOI: https://doi.org/10.1038/nrn3241, PMID: 22595786

Chauvette S, Volgushev M, Timofeev I. 2010. Origin of active states in local neocortical networks during slow sleep oscillation. *Cerebral Cortex* **20**:2660–2674. DOI: https://doi.org/10.1093/cercor/bhq009, PMID: 20200108

Cirelli C, Faraguna U, Tononi G. 2006. Changes in brain gene expression after long-term sleep deprivation. *Journal of Neurochemistry* **98**:1632–1645. DOI: https://doi.org/10.1111/j.1471-4159.2006.04058.x, PMID: 16923172

Cobley JN, Fiorello ML, Bailey DM. 2018. 13 reasons why the brain is susceptible to oxidative stress. *Redox Biology* **15**:490–503. DOI: https://doi.org/10.1016/j.redox.2018.01.008, PMID: 29413961

Daan S, Beersma DG, Borbély AA. 1984. Timing of human sleep: recovery process gated by a circadian pacemaker. *American Journal of Physiology-Regulatory, Integrative and Comparative Physiology* **246**:R161–R183. DOI: https://doi.org/10.1152/ajpregu.1984.246.2.R161, PMID: 6696142

Fisher SP, Cui N, McKillop LE, Gemignani J, Bannerman DM, Oliver PL, Peirson SN, Vyazovskiy VV. 2016. Stereotypic wheel running decreases cortical activity in mice. *Nature Communications* **7**:ncomms13138. DOI: https://doi.org/10.1038/ncomms13138

Frank MG, Heller HC. 2019. Handbook of Experimental Pharmacology. In: Landolt HP, Dijk DJ (Eds). *The Function(s) of Sleep*. Springer. p. 3–34. DOI: https://doi.org/10.1007/164_2018_140

Franken P, Dijk DJ, Tobler I, Borbely AA. 1991a. Sleep deprivation in rats: effects on EEG power spectra, vigilance states, and cortical temperature. *American Journal of Physiology-Regulatory, Integrative and Comparative Physiology* **261**:R198–R208. DOI: https://doi.org/10.1152/ajpregu.1991.261.1.R198

Franken P, Tobler I, Borbély AA. 1991b. Sleep homeostasis in the rat: simulation of the time course of EEG slow-wave activity. *Neuroscience Letters* **130**:141–144. DOI: https://doi.org/10.1016/0304-3940(91)90382-4, PMID: 1795873

Funk CM, Honjoh S, Rodriguez AV, Cirelli C, Tononi G. 2016. Local slow waves in superficial layers of primary cortical Areas during REM sleep. *Current Biology* **26**:396–403. DOI: https://doi.org/10.1016/j.cub.2015.11.062, PMID: 26804554

González-Rueda A, Pedrosa V, Feord RC, Clopath C, Paulsen O. 2018. Activity-Dependent downscaling of subthreshold synaptic inputs during Slow-Wave-Sleep-like activity in Vivo. *Neuron* **97**:1244–1252. DOI: https://doi.org/10.1016/j.neuron.2018.01.047, PMID: 29503184

Graupner M, Wallisch P, Ostojic S. 2016. Natural firing patterns imply low sensitivity of synaptic plasticity to spike timing compared with firing rate. *The Journal of Neuroscience* **36**:11238–11258. DOI: https://doi.org/10.1523/JNEUROSCI.0104-16.2016, PMID: 27807166

Grosmark AD, Mizuseki K, Pastalkova E, Diba K, Buzsáki G. 2012. REM sleep reorganizes hippocampal excitability. *Neuron* **75**:1001–1007. DOI: https://doi.org/10.1016/j.neuron.2012.08.015, PMID: 22998869

Guillaumin MCC, McKillop LE, Cui N, Fisher SP, Foster RG, de Vos M, Peirson SN, Achermann P, Vyazovskiy VV. 2018. Cortical region–specific sleep homeostasis in mice: effects of time of day and waking experience. *Sleep* **41**:zsy079. DOI: https://doi.org/10.1093/sleep/zsy079

Hastings MH, Maywood ES, Brancaccio M. 2019. The mammalian circadian timing system and the suprachiasmatic nucleus as its pacemaker. *Biology* **8**:13. DOI: https://doi.org/10.3390/biology8010013, PMID: 30862123

Hengen KB, Lambo ME, Van Hooser SD, Katz DB, Turrigiano GG. 2013. Firing rate homeostasis in visual cortex of freely behaving rodents. *Neuron* **80**:335–342. DOI: https://doi.org/10.1016/j.neuron.2013.08.038, PMID: 24139038

Hengen KB, Torrado Pacheco A, McGregor JN, Van Hooser SD, Turrigiano GG. 2016. Neuronal firing rate homeostasis is inhibited by sleep and promoted by wake. *Cell* **165**:180–191. DOI: https://doi.org/10.1016/j.cell.2016.01.046, PMID: 26997481

Hoekstra MM, Emmenegger Y, Hubbard J, Franken P. 2019. Cold-inducible RNA-binding protein (CIRBP) adjusts clock-gene expression and REM-sleep recovery following sleep deprivation. *eLife* **8**:e43400. DOI: https://doi.org/10.7554/eLife.43400, PMID: 30720431

Hsu D, Beggs JM. 2006. Neuronal avalanches and criticality: a dynamical model for homeostasis. *Neurocomputing* **69**:1134–1136. DOI: https://doi.org/10.1016/j.neucom.2005.12.060

Huber R, Deboer T, Tobler I. 2000a. Effects of sleep deprivation on sleep and sleep EEG in three mouse strains: empirical data and simulations. *Brain Research* **857**:8–19. DOI: https://doi.org/10.1016/S0006-8993(99)02248-9, PMID: 10700548

Huber R, Deboer T, Tobler I. 2000b. Topography of EEG dynamics after sleep deprivation in mice. *Journal of Neurophysiology* **84**:1888–1893. DOI: https://doi.org/10.1152/jn.2000.84.4.1888, PMID: 11024081

Huber R, Ghilardi MF, Massimini M, Tononi G. 2004. Local sleep and learning. *Nature* **430**:78–81. DOI: https://doi.org/10.1038/nature02663, PMID: 15184907

Kajikawa Y, Schroeder CE. 2011. How local is the local field potential? *Neuron* **72**:847–858. DOI: https://doi.org/10.1016/j.neuron.2011.09.029, PMID: 22153379

Kattler H, Dijk DJ, Borbély AA. 1994. Effect of unilateral somatosensory stimulation prior to sleep on the sleep EEG in humans. *Journal of Sleep Research* **3**:159–164. DOI: https://doi.org/10.1111/j.1365-2869.1994.tb00123.x, PMID: 10607121

Kempf A, Song SM, Talbot CB, Miesenböck G. 2019. A potassium channel β-subunit couples mitochondrial electron transport to sleep. *Nature* **568**:230–234. DOI: https://doi.org/10.1038/s41586-019-1034-5, PMID: 30894743

Krueger JM, Rector DM, Roy S, Van Dongen HP, Belenky G, Panksepp J. 2008. Sleep as a fundamental property of neuronal assemblies. *Nature Reviews Neuroscience* **9**:910–919. DOI: https://doi.org/10.1038/nrn2521, PMID: 18985047

Krueger JM, Tononi G. 2011. Local use-dependent sleep; synthesis of the new paradigm. *Current Topics in Medicinal Chemistry* **11**:2490–2492. DOI: https://doi.org/10.2174/156802611797470330, PMID: 21906015

Kültz D. 2005. Molecular and evolutionary basis of the cellular stress response. *Annual Review of Physiology* **67**:225–257. DOI: https://doi.org/10.1146/annurev.physiol.67.040403.103635, PMID: 15709958

Kunz H, Achermann P. 2003. Simulation of circadian rhythm generation in the suprachiasmatic nucleus with locally coupled self-sustained oscillators. *Journal of Theoretical Biology* **224**:63–78. DOI: https://doi.org/10.1016/S0022-5193(03)00141-3, PMID: 12900204

Lagarias JC, Reeds JA, Wright MH, Wright PE. 1998. Convergence properties of the nelder–mead simplex method in low dimensions. *SIAM Journal on Optimization* **9**:112–147. DOI: https://doi.org/10.1137/S1052623496303470

Lappalainen J, Herpich J, Tetzlaff C. 2019. A theoretical framework to derive simple, Firing-Rate-Dependent mathematical models of synaptic plasticity. *Frontiers in Computational Neuroscience* **13**:26. DOI: https://doi.org/10.3389/fncom.2019.00026, PMID: 31133837

Levenstein D, Watson BO, Rinzel J, Buzsáki G. 2017. Sleep regulation of the distribution of cortical firing rates. *Current Opinion in Neurobiology* **44**:34–42. DOI: https://doi.org/10.1016/j.conb.2017.02.013, PMID: 28288386

Liu C, Weaver DR, Strogatz SH, Reppert SM. 1997. Cellular construction of a circadian clock: period determination in the suprachiasmatic nuclei. *Cell* **91**:855–860. DOI: https://doi.org/10.1016/S0092-8674(00)80473-0, PMID: 9413994

Liu ZW, Faraguna U, Cirelli C, Tononi G, Gao XB. 2010. Direct evidence for wake-related increases and sleep-related decreases in synaptic strength in rodent cortex. *Journal of Neuroscience* **30**:8671–8675. DOI: https://doi.org/10.1523/JNEUROSCI.1409-10.2010, PMID: 20573912

Mackiewicz M, Shockley KR, Romer MA, Galante RJ, Zimmerman JE, Naidoo N, Baldwin DA, Jensen ST, Churchill GA, Pack AI. 2007. Macromolecule biosynthesis: a key function of sleep. *Physiological Genomics* **31**:441–457. DOI: https://doi.org/10.1152/physiolgenomics.00275.2006, PMID: 17698924

Massimini M, Huber R, Ferrarelli F, Hill S, Tononi G. 2004. The sleep slow oscillation as a traveling wave. *Journal of Neuroscience* **24**:6862–6870. DOI: https://doi.org/10.1523/JNEUROSCI.1318-04.2004, PMID: 15295020

McKillop LE, Fisher SP, Cui N, Peirson SN, Foster RG, Wafford KA, Vyazovskiy VV. 2018. Effects of aging on cortical neural dynamics and local sleep homeostasis in mice. *The Journal of Neuroscience* **38**:3911–3928. DOI: https://doi.org/10.1523/JNEUROSCI.2513-17.2018, PMID: 29581380

Meisel C, Olbrich E, Shriki O, Achermann P. 2013. Fading signatures of critical brain dynamics during sustained wakefulness in humans. *Journal of Neuroscience* **33**:17363–17372. DOI: https://doi.org/10.1523/JNEUROSCI.1516-13.2013, PMID: 24174669

Miyawaki H, Watson BO, Diba K. 2019. Neuronal firing rates diverge during REM and homogenize during non-REM. *Scientific Reports* **9**:689. DOI: https://doi.org/10.1038/s41598-018-36710-8, PMID: 30679509

Miyawaki H, Diba K. 2016. Regulation of hippocampal firing by network oscillations during sleep. *Current Biology* **26**:893–902. DOI: https://doi.org/10.1016/j.cub.2016.02.024, PMID: 26972321

Murphy M, Huber R, Esser S, Riedner BA, Massimini M, Ferrarelli F, Ghilardi MF, Tononi G. 2011. The cortical topography of local sleep. *Current Topics in Medicinal Chemistry* **11**:2438–2446. DOI: https://doi.org/10.2174/156802611797470303, PMID: 21906021

Ness TV, Remme MW, Einevoll GT. 2016. Active subthreshold dendritic conductances shape the local field potential. *The Journal of Physiology* **594**:3809–3825. DOI: https://doi.org/10.1113/JP272022, PMID: 27079755

O'Leary T, Williams AH, Franci A, Marder E. 2014. Cell types, network homeostasis, and pathological compensation from a biologically plausible ion channel expression model. *Neuron* **82**:809–821. DOI: https://doi.org/10.1016/j.neuron.2014.04.002, PMID: 24853940

Okun M, Steinmetz N, Cossell L, Iacaruso MF, Ko H, Barthó P, Moore T, Hofer SB, Mrsic-Flogel TD, Carandini M, Harris KD. 2015. Diverse coupling of neurons to populations in sensory cortex. *Nature* **521**:511–515. DOI: https://doi.org/10.1038/nature14273, PMID: 25849776

Pearlmutter BA, Houghton CJ. 2009. A new hypothesis for sleep: tuning for criticality. *Neural Computation* **21**:1622–1641. DOI: https://doi.org/10.1162/neco.2009.05-08-787, PMID: 19191602

Priesemann V, Valderrama M, Wibral M, Le Van Quyen M. 2013. Neuronal avalanches differ from wakefulness to deep sleep–evidence from intracranial depth recordings in humans. *PLOS Computational Biology* **9**:e1002985. DOI: https://doi.org/10.1371/journal.pcbi.1002985, PMID: 23555220

Qiu MH, Chen MC, Lu J. 2015. Cortical neuronal activity does not regulate sleep homeostasis. *Neuroscience* **297**:211–218. DOI: https://doi.org/10.1016/j.neuroscience.2015.03.070, PMID: 25864961

Quiroga RQ, Nadasdy Z, Ben-Shaul Y. 2004. Unsupervised spike detection and sorting with wavelets and superparamagnetic clustering. *Neural Computation* **16**:1661–1687. DOI: https://doi.org/10.1162/089976604774201631, PMID: 15228749

Rattenborg NC, Lima SL, Lesku JA. 2012. Sleep locally, act globally. *The Neuroscientist* **18**:533–546. DOI: https://doi.org/10.1177/1073858412441086, PMID: 22572533

Rector DM, Schei JL, Van Dongen HP, Belenky G, Krueger JM. 2009. Physiological markers of local sleep. *European Journal of Neuroscience* **29**:1771–1778. DOI: https://doi.org/10.1111/j.1460-9568.2009.06717.x, PMID: 19473232

Reimann MW, Anastassiou CA, Perin R, Hill SL, Markram H, Koch C. 2013. A biophysically detailed model of neocortical local field potentials predicts the critical role of active membrane currents. *Neuron* **79**:375–390. DOI: https://doi.org/10.1016/j.neuron.2013.05.023, PMID: 23889937

Reimund E. 1994. The free radical flux theory of sleep. *Medical Hypotheses* **43**:231–233. DOI: https://doi.org/10.1016/0306-9877(94)90071-X, PMID: 7838006

Rodriguez AV, Funk CM, Vyazovskiy VV, Nir Y, Tononi G, Cirelli C. 2016. Why does sleep Slow-Wave activity increase after extended wake? assessing the effects of increased cortical firing during wake and sleep. *The Journal of Neuroscience* **36**:12436–12447. DOI: https://doi.org/10.1523/JNEUROSCI.1614-16.2016, PMID: 27927960

Rusterholz T, Achermann P. 2011. Topographical aspects in the dynamics of sleep homeostasis in young men: individual patterns. *BMC Neuroscience* **12**:84. DOI: https://doi.org/10.1186/1471-2202-12-84, PMID: 21846365

Saberi-Moghadam S, Simi A, Setareh H, Mikhail C, Tafti M. 2018. In vitro cortical network firing is homeostatically regulated: a model for sleep regulation. *Scientific Reports* **8**:6297. DOI: https://doi.org/10.1038/s41598-018-24339-6, PMID: 29674729

Sanchez-Vives MV, Mattia M. 2014. Slow wave activity as the default mode of the cerebral cortex. *Archives Italiennes De Biologie* **152**:147–155. DOI: https://doi.org/10.12871/000298292014239, PMID: 25828686

Scharf MT, Naidoo N, Zimmerman JE, Pack AI. 2008. The energy hypothesis of sleep revisited. *Progress in Neurobiology* **86**:264–280. DOI: https://doi.org/10.1016/j.pneurobio.2008.08.003, PMID: 18809461

Seibt J, Frank MG. 2019. Primed to sleep: the dynamics of synaptic plasticity across brain states. *Frontiers in Systems Neuroscience* **13**:2. DOI: https://doi.org/10.3389/fnsys.2019.00002

Slomowitz E, Styr B, Vertkin I, Milshtein-Parush H, Nelken I, Slutsky M, Slutsky I. 2015. Interplay between population firing stability and single neuron dynamics in hippocampal networks. *eLife* **4**:e04378. DOI: https://doi.org/10.7554/eLife.04378

Steriade M, Nuñez A, Amzica F. 1993a. Intracellular analysis of relations between the slow (< 1 hz) neocortical oscillation and other sleep rhythms of the electroencephalogram. *The Journal of Neuroscience* **13**:3266–3283. DOI: https://doi.org/10.1523/JNEUROSCI.13-08-03266.1993, PMID: 8340807

Steriade M, Nuñez A, Amzica F. 1993b. A novel slow (< 1 hz) oscillation of neocortical neurons in vivo: depolarizing and hyperpolarizing components. *The Journal of Neuroscience* **13**:3252–3265. DOI: https://doi.org/10.1523/JNEUROSCI, PMID: 8340806

Steriade M, Timofeev I, Grenier F. 2001. Natural waking and sleep states: a view from inside neocortical neurons. *Journal of Neurophysiology* **85**:1969–1985. DOI: https://doi.org/10.1152/jn.2001.85.5.1969, PMID: 11353014

Styr B, Gonen N, Zarhin D, Ruggiero A, Atsmon R, Gazit N, Braun G, Frere S, Vertkin I, Shapira I, Harel M, Heim LR, Katsenelson M, Rechnitz O, Fadila S, Derdikman D, Rubinstein M, Geiger T, Ruppin E, Slutsky I. 2019. Mitochondrial regulation of the hippocampal firing rate set point and seizure susceptibility. *Neuron* **102**:1009–1024. DOI: https://doi.org/10.1016/j.neuron.2019.03.045, PMID: 31047779

Timofeev I, Chauvette S. 2017. Sleep slow oscillation and plasticity. *Current Opinion in Neurobiology* **44**:116–126. DOI: https://doi.org/10.1016/j.conb.2017.03.019, PMID: 28453998

Tobler I, Deboer T, Fischer M. 1997. Sleep and sleep regulation in normal and prion protein-deficient mice. *The Journal of Neuroscience* **17**:1869–1879. DOI: https://doi.org/10.1523/JNEUROSCI.17-05-01869.1997, PMID: 9030645

Todorova R, Zugaro M. 2019. Isolated cortical computations during Delta waves support memory consolidation. *Science* **366**:377–381. DOI: https://doi.org/10.1126/science.aay0616, PMID: 31624215

Tononi G, Cirelli C. 2003. Sleep and synaptic homeostasis: a hypothesis. *Brain Research Bulletin* **62**:143–150. DOI: https://doi.org/10.1016/j.brainresbull.2003.09.004, PMID: 14638388

Tononi G, Cirelli C. 2014. Sleep and the price of plasticity: from synaptic and cellular homeostasis to memory consolidation and integration. *Neuron* **81**:12–34. DOI: https://doi.org/10.1016/j.neuron.2013.12.025, PMID: 24411729

Turrigiano G. 2011. Too many cooks? intrinsic and synaptic homeostatic mechanisms in cortical circuit refinement. *Annual Review of Neuroscience* **34**:89–103. DOI: https://doi.org/10.1146/annurev-neuro-060909-153238, PMID: 21438687

Vergara RC, Jaramillo-Riveri S, Luarte A, Moënne-Loccoz C, Fuentes R, Couve A, Maldonado PE. 2019. The energy homeostasis principle: neuronal energy regulation drives local network dynamics generating behavior. *Frontiers in Computational Neuroscience* **13**:49. DOI: https://doi.org/10.3389/fncom.2019.00049, PMID: 31396067

Vyazovskiy VV, Achermann P, Tobler I. 2007. Sleep homeostasis in the rat in the light and dark period. *Brain Research Bulletin* **74**:37–44. DOI: https://doi.org/10.1016/j.brainresbull.2007.05.001, PMID: 17683787

Vyazovskiy VV, Cirelli C, Pfister-Genskow M, Faraguna U, Tononi G. 2008. Molecular and electrophysiological evidence for net synaptic potentiation in wake and depression in sleep. *Nature Neuroscience* **11**:200–208. DOI: https://doi.org/10.1038/nn2035, PMID: 18204445

Vyazovskiy VV, Olcese U, Lazimy YM, Faraguna U, Esser SK, Williams JC, Cirelli C, Tononi G. 2009. Cortical firing and sleep homeostasis. *Neuron* **63**:865–878. DOI: https://doi.org/10.1016/j.neuron.2009.08.024, PMID: 19778514

Vyazovskiy VV, Olcese U, Hanlon EC, Nir Y, Cirelli C, Tononi G. 2011. Local sleep in awake rats. *Nature* **472**:443–447. DOI: https://doi.org/10.1038/nature10009, PMID: 21525926

Vyazovskiy VV, Cui N, Rodriguez AV, Funk C, Cirelli C, Tononi G. 2014. The dynamics of cortical neuronal activity in the first minutes after spontaneous awakening in rats and mice. *Sleep* **37**:1337–1347. DOI: https://doi.org/10.5665/sleep.3926, PMID: 25083014

Vyazovskiy VV. 2015. Sleep, recovery, and metaregulation: explaining the benefits of sleep. *Nature and Science of Sleep* **7**:171–184. DOI: https://doi.org/10.2147/NSS.S54036, PMID: 26719733

Vyazovskiy VV, Delogu A. 2014. NREM and REM sleep: complementary roles in recovery after wakefulness. *The Neuroscientist : A Review Journal Bringing Neurobiology, Neurology and Psychiatry* **20**:203–219. DOI: https://doi.org/10.1177/1073858413518152, PMID: 24598308

Vyazovskiy VV, Harris KD. 2013. Sleep and the single neuron: the role of global slow oscillations in individual cell rest. *Nature Reviews Neuroscience* **14**:443–451. DOI: https://doi.org/10.1038/nrn3494

Vyazovskiy VV, Tobler I. 2008. Handedness leads to interhemispheric EEG asymmetry during sleep in the rat. *Journal of Neurophysiology* **99**:969–975. DOI: https://doi.org/10.1152/jn.01154.2007

Wang X, Michaelis EK. 2010. Selective neuronal vulnerability to oxidative stress in the brain. *Frontiers in Aging Neuroscience* **2**:12. DOI: https://doi.org/10.3389/fnagi.2010.00012, PMID: 20552050

Watson BO, Levenstein D, Greene JP, Gelinas JN, Buzsáki G. 2016. Network homeostasis and state dynamics of neocortical sleep. *Neuron* **90**:839–852. DOI: https://doi.org/10.1016/j.neuron.2016.03.036, PMID: 27133462

Werth E, Achermann P, Borbély AA. 1996. Brain topography of the human sleep EEG: antero-posterior shifts of spectral power. *Neuroreport* **8**:123–127. DOI: https://doi.org/10.1097/00001756-199612200-00025, PMID: 9051765

Zavada A, Strijkstra AM, Boerema AS, Daan S, Beersma DG. 2009. Evidence for differential human slow-wave activity regulation across the brain. *Journal of Sleep Research* **18**:3–10. DOI: https://doi.org/10.1111/j.1365-2869.2008.00696.x, PMID: 19021858

Zucca S, Pasquale V, Lagomarsino de Leon Roig P, Panzeri S, Fellin T. 2019. Thalamic drive of cortical Parvalbumin-Positive interneurons during down states in anesthetized mice. *Current Biology* **29**:1481–1490. DOI: https://doi.org/10.1016/j.cub.2019.04.007, PMID: 31031117